Immunosuppression by mutated calreticulin released from malignant cells

Peng Liu[1-4*], Liwei Zhao[1-5*], Friedemann Loos[1-4], Caroline Marty[5-7], Wei Xie[1-4], Isabelle Martins[1-4], Sylvie Lachkar[1-4], Bo Qu[7-9], Emmanuelle Waeckel-Énée[4,10,11], Isabelle Plo[5-7], William Vainchenker[5-7], Franck Perez[12], David Rodriguez[13], Carlos López-Otin[1-4,13], Peter van Endert[4,10,11] Laurence Zitvogel[7-9], Oliver Kepp[1-4], and Guido Kroemer[1-4,14-17]

[1]*Metabolomics and Cell Biology Platforms, Gustave Roussy Comprehensive Cancer Institute, Villejuif, France;*
[2]*Equipe 11 labellisée Ligue contre le Cancer, Centre de Recherche des Cordeliers, INSERM UMR 1138, Paris, France;*
[3]*Sorbonne Université, Paris, France;*
[4]*Université of Paris, Paris, France;*
[5]*Université Paris-Saclay, Villejuif, France;*
[6]*INSERM, UMR 1170, Villejuif, France;*
[7]*Gustave Roussy Comprehensive Cancer Center, Villejuif, France;*
[8]*INSERM, U1015, Villejuif, France;*
[9]*Center of Clinical Investigations, CIC1428, Villejuif, France;*
[10]*INSERM, U1151, Paris, France;*
[11]*CNRS UMR8253, Paris, France;*
[12]*Cell Biology and Cancer Unit, Institut Curie, PSL Research University, CNRS, Paris, France;*
[13]*Departamento de Bioquímica y Biología Molecular, Facultad de Medicina, Instituto Universitario de Oncología (IUOPA), Centro de Investigación Biomédica en Red de Cáncer (CIBERONC),Universidad de Oviedo, 33006 Oviedo, Spain*
[14]*Suzhou Institute for Systems Medicine, Chinese Academy of Sciences, Suzhou, China；*
[15]*Karolinska Institutet, Department of Women's and Children's Health, Stockholm, Sweden;*
[16]*Pôle de Biologie, Hôpital Européen Georges Pompidou, AP-HP, Paris, France.*
[17]*Lead Contact*

*contributed equally

Correspondence: Oliver KEPP captain.olsen@gmail.com
Guido KROEMER kroemer@orange.fr

Key words: calreticulin; ICD, immunogenic cell death; immunosuppression; phagocytosis

Running title: CALR mutation-elicited immunosuppression

Summary

Mutations affecting exon 9 of the *CALR* gene lead to the generation of a C-terminally modified calreticulin (CALR) protein that lacks the KDEL endoplasmic reticulum (ER) retention signal and consequently mislocalizes outside of the ER where it activates the thrombopoietin receptor in a cell-autonomous fashion, thus driving myeloproliferative diseases. Here we used the 'retention using selective hooks' (RUSH) assay to monitor the trafficking of CALR. We found that exon 9-mutated CALR was released from cells in response to the biotin-mediated detachment from its ER-localized hook, *in vitro* and *in vivo*. Cellular CALR release was confirmed in suitable mouse models bearing exon 9-mutated hematopoietic systems or tumors. Extracellular CALR mediated immunomodulatory effects and inhibited the phagocytosis of dying cancer cells by dendritic cells, thereby suppressing antineoplastic immune responses elicited by chemotherapeutic agents or by PD-1 blockade. Altogether, our results demonstrate paracrine immunosuppressive effects for exon 9-mutated CALR.

Introduction

Calreticulin (CALR) is a highly abundant calcium-binding chaperone that mostly resides in the endoplasmic reticulum (ER) where it is retained through its C-terminal KDEL retention sequence (Michalak et al., 2009). In cancer cells experiencing a peculiar ER stress response elicited by therapeutic agents (with activation of kinases that phosphorylate eIF2α but no activation of the ATG6 and IRE1a-XBP1 arms of the unfolded stress response), CALR can translocate from the ER to the plasma membrane (Garg et al., 2012; Obeid et al., 2007; Panaretakis et al., 2009; van Vliet et al., 2017). Moreover, macrophages can expose CALR on the cell surface following the Toll-like receptor 4-stimulated phosphorylation of CALR by Bruton's tyrosine kinase (Feng et al., 2015). When present on the cell surface, CALR acts as an 'eat me' signal that facilitates the recognition of stressed cells by phagocytes expressing the CALR receptor CD91 (Brown and Neher, 2012; Gardai et al., 2003). Thus, CALR acts as a bridge to interact with specific asialoglycans (Feng et al., 2018) or phosphatidylserine molecules found on the cell surface (Wijeyesakere et al., 2016) and its interacting partners C1q, thrombospondin and membrane-bound CD91 (Michalak et al., 2009). Of note, it appears that this type of innate immune recognition can facilitate the transfer of tumor-associated antigens expressed by malignant cells to dendritic cells (DC), thus favoring MHC class I-restricted antigen cross-presentation and induction of cancer-specific cytotoxic T lymphocytes (Kroemer et al., 2013). Thus, CALR exposure is an important hallmark of 'immunogenic cell death' (ICD), in which stressed and dying cancer cells stimulate their phagocytic uptake by DC, then induce DC maturation/antigen presentation, and ultimately favor the induction of T cell-mediated anticancer immune responses (Galluzzi et al., 2017).

In specific circumstances, soluble CALR protein can be released from cells. This has been observed after chemotherapy in the context of massive cell death (Olivieri et al., 1990), as well upon activation of macrophages (Byrne et al., 2013). Soluble CALR protein has multiple effects on the microenvironment, thus stimulating the healing of skin wounds (Greives et al., 2012) and affecting the phenotype and function of macrophages (Osman et al., 2017). CALR can be digested by proteases such as neutrophil elastase to generate a factor called 'vasostatin' that inhibits angiogenesis (Mans et al., 2012). The systemic injection of CALR fragments into mice can also stimulate the expansion of myeloid derived suppressor cells (MDSC) (He et al., 2017) or that of immunosuppressive B cells (Hong et al., 2013).

Mutations in *CALR* occur in approximately 30% of patients with myeloproliferative neoplasms (MPNs) such as essential thrombocythemia and myelofibrosis (Klampfl et al., 2013; Nangalia et al., 2013). Typically, such mutations occur in a heterozygous fashion within exon 9 as a 52-base pair deletion at residues 1092 to 1142 (*CALRdel52* representative of type 1 mutants) or as a 5-base pair insertion between residues 1154 and 1155 (*CALRins5* representative of type 2 mutants), yielding proteins with a modified C-terminus that lack the KDEL ER retention signal (Grinfeld et al., 2018). Introduction of either of these two mutations into the bone marrow of mice is sufficient to cause a specific amplification of megakaryocytes and platelet production, proving the cause-effect relationship between CALR mutation and oncogenesis (Marty et al., 2016). Mechanistically, the mutant CALR proteins escapes from the ER and can be secreted from cells (Arshad and Cresswell, 2018; Garbati et al., 2016; Han et al., 2016). Outside of the ER, mutant CALR proteins interact with, and specifically activate, the thrombopoietin receptor (MPL) to induce activation of the Janus kinase 2 (JAK2) and signal transducer and activator of transcription 1/3/5 (Chachoua et al., 2016; Elf et al., 2018; Marty et al., 2016). The combination

with additional oncogenic drivers (such as the epigenetic regulators ASXL1 or EZH2 as well as other genes involved in splicing or signaling), can modify the MPN phenotype leading to dysplastic features with progression to myelofibrosis or eventually acute myeloid leukemia (Vainchenker and Kralovics, 2017).

Of note, the oncogenic activity of exon 9-mutated CALR has been attributed to essentially autocrine signals leading to MPL activation in, or at the cell surface of, the mutated cell itself (Araki and Komatsu, 2017). However, no paracrine MPL stimulation has been detected in non-mutated cells cultured with mutated cells or their conditioned media, likely because MPL must be in an immature glycosylated form to bind CALR (Araki et al., 2016; Han et al., 2016). Here, we investigated how exon 9-mutated CALR is secreted and whether it mediates extracellular effects independent from MPL. We used a series of chemical biology and molecular biology tools to demonstrate that exon 9-mutated CALR is released from cells, accumulating in the extracellular space and binding to other cells. Soluble CALR protein then acts as a decoy receptor, preventing the uptake of CALR-exposing cells by DC, thus mediating prominent immunosuppressive effects.

Results

Secretion of mutant CALR. We recently developed a chemical biology tool, the 'retention using selective hooks' (RUSH) system in which a streptavidin protein can be placed in distinct subcellular locations to sequestrate proteins fused to a streptavidin-binding peptide (SBP) (Boncompain et al., 2012; Liu et al., 2017; Zhao et al., 2018). We used the RUSH technology to explore the subcellular localization and transport of wild type (wt) CALR and two representative CALR mutants (mt1CALR representative of type 1 mutants such as CALRdel52; mt2CALR representative of type 2 mutants such as CALRins5) while comparing them to that of a secretable version of GFP. wtCALR, mt1CALR and mt2CALR were N-terminally coupled to an SBP-GFP fusion protein to generate the chimeric proteins SBP-GFP-wtCALR, SBP-GFP-mt1CALR and SBP-GFP-mt2CALR, all of which carried the ER translocation signal of CALR at their N-termini to ensure their correct subcellular localization (**Fig. S1A**). Genes coding for these fusion products were stably transfected into U2OS osteosarcoma cells expressing the streptavidin 'hook' in the ER due to the C-terminal addition of the ER retention signal KDEL (**Fig. 1A**). When biotin was added, the ER-sessile GFP signal was locally maintained for SBP-GFP-wtCALR (**Fig. 1C,F; Fig. S1B; Video. S1**) but was lost from the cells within a few hours with similar kinetics for SBP-GFP-mt1CALR and SBP-GFP-mt2CALR, as well as for the control SBP-GFP chimera lacking a CALR moiety (**Fig. 1A-F; Fig. S1C,D; Video. S2,3**).

To determine the mechanisms accounting for the release of SBP-GFP-mt1/2CALR mutants from biotin-treated cells, we determined the effects of brefeldin A (BFA), an inhibitor of conventional protein secretion, on the system, while we simultaneously measured the co-localization of the GFP signal with the Golgi marker GALT1 (**Fig. 1G**). BFA, which disrupted the Golgi apparatus, inhibited the biotin-induced cellular release of SBP-GFP-mt1CALR and SBP-GFP-mt2CALR

(**Fig. S1C,D, Video. S4-6**). Moreover, upon addition of biotin without BFA, SBP-GFP-mt1CALR and SBP-GFP-mt2CALR transiently colocalized with GALT1 (with a peak around ~30 min post-biotin) (**Fig. 1H-J, Fig. S1E,F**), in line with the idea that CALR mutants are secreted via the Golgi, through a canonical pathway. The transient colocalization of SBP-GFP-mt1CALR and SBP-GFP-mt2CALR with the Golgi apparatus was confirmed by staining of the cells with antibodies specific for Golgi-sessile proteins (data not shown). Moreover, pretreatment with BFA prevented the biotin-induced release of SBP-GFP-mt1CALR and SBP-GFP-mt2CALR into the culture supernatant, as determined by immunoblot analyses (**Fig. 2A,B**) or ELISA (**Fig. 2C-E**). Of note, in this system, the concentration of mutant CALR released from the ER in response to biotin reached ~50 times higher levels than that of wtCALR (**Fig. 2C-E**). All these results, which were obtained in U2OS cells, could be recapitulated in another cell line, namely, human cervical carcinoma HeLa cells (**Fig. S2**). Moreover, they reflect the *in vivo* pathophysiology of CALR mutations occurring in the context of MPN (Vainchenker and Kralovics, 2017). Thus, ELISA-detectable CALR levels were increased in the plasma of patients with essential thrombocythemia or myelofibrosis as compared to age-matched controls (**Fig. 2F**). Of note, immunofluorescence staining revealed a higher level of cell surface-bound CALR, both for circulating monocytes (**Fig. 2G, Fig. S3A**) and lymphocytes (**Fig. 2H, Fig. S3B**) from patients bearing CALR mutations.

In conclusion, in contrast to wtCALR, mutated CALR is not withhold in the ER but rather is released from cells through BFA-inhibitable secretion. CALR then binds to other cells or accumulates in the extracellular place including the plasma. These data are consistent with previous publications (Arshad and Cresswell, 2018; Garbati et al., 2016; Han et al., 2016).

Inhibition of phagocytosis by excess amount of soluble CALR. Surface-bound CALR is well known to bridge saturable binding sites (such as externalized phosphatidylserine residues and tumor-associated asialoglycans, C1q, thrombospondin etc.) on phagocytes and their preys, thereby favoring phagocytosis (Feng et al., 2018; Krysko et al., 2018). We reasoned that excessive soluble CALR might saturate such binding sites, thereby inhibiting phagocytosis. Indeed, when $CD11c^+$ bone marrow-derived dendritic cells (BMDC) were cocultured with fluorophore-labelled (CellTracker Orange, CMTMR) cancer cells treated with oxaliplatin (which causes CALR exposure, **Fig. S3C,D**), double-positive ($CD11c^+$ $CMTRMR^+$) structures indicative of phagocytosis were formed in a temperature-dependent fashion. Addition of excess amounts of recombinant CALR protein (that saturated binding sites on the BMDC surface, **Fig. S3E-H**) inhibited this process that was detectable by conventional flow cytometry (**Fig. 3A,B**) or imaging flow cytometry (**Fig. 3C,D**). These results were obtained with a practically endotoxin-free soluble CALR protein (Obeid et al., 2007) and were not altered by the endotoxin-neutralizing antibiotic polymyxin B (**Fig. 3E**). Moreover, soluble CALR also inhibited the phagocytosis of life cells engineered to constitutively express CALR on their surface (**Fig. S3I,J**). The CALR-mediated inhibition of phagocytosis results could be recapitulated *in vivo*, by intravenously injecting recombinant CALR protein or by using conditional knock-in mice expressing mtCALR in bone marrow cells (*CALRdel52*) (Marty et al., 2016). These two manipulations led to an equivalent increase in free plasma CALR concentrations (**Fig. 3F,G**). When PKH26-fluorescent labeled MCA205 fibrosarcoma cells treated with oxaliplatin (to cause CALR exposure) (Obeid et al., 2007) were injected into the spleen of anaesthetized mice, a substantial fraction of the cancer cells (around 8%) were rapidly (3 h post-injection) engulfed by $CD11c^+$ dendritic cells (DC), as determined by immunofluorescence and cytofluorometry. This engulfment process was not observed for untreated MCA205 cells and was inhibited in conditions in which soluble CALR

levels were augmented (**Fig. 3H-J**). Of note, soluble CALR failed to reduce the uptake of bacterial particles by peritoneal macrophages, indicating that soluble CALR does not suppress phagocytosis in a non-specific fashion (**Fig. S3K,L**).

In conclusion, soluble CALR inhibits phagocytosis of CALR-exposing cells both *in vitro* and *in vivo*.

Immunosuppressive activity of systemically elevated soluble CALR. In the context of immunogenic cell death (ICD), CALR-dependent phagocytosis of dying cancer cells is required for the induction of protective antitumor immune responses (Obeid et al., 2007). To investigate whether excess soluble CALR inhibiting phagocytosis (see **Fig. 3B,D,J**) would prevent anticancer immunity, we injected recombinant CALR protein or vehicle (PBS) intravenously, as we vaccinated the mice by subcutaneous injection of either PBS alone or dying MCA205 cells (killed with the ICD inducer mitoxantrone, MTX). One week later, the mice were rechallenged with live MCA205 cells that were inoculated into the opposite flank (**Fig. 4A**). In control conditions, MTX-killed MCA205 induced a protective immune response, precluding the later outgrowth of live cancer cells *in vivo*. This vaccination effect was suppressed by systemic administration of soluble CALR protein along with the ICD vaccine (**Fig. 4B,C**). Alternatively, we increased soluble CALR protein levels detectable in the plasma by transferring the bone marrow from mice expressing mtCALR (*CALRdel52*) into lethally irradiated recipients, waited for the reconstitution of the hematopoietic system and then performed vaccination experiments (**Fig. 4D**). In conditions in which soluble CALR was elevated in the plasma (i.e. in bone marrow chimeras having received grafts from CALRdel52, not WT, donors) (**Fig. 4E)**, vaccination with MTX-killed cancer cells failed, contrasting with the effective protection of naïve animals or mice bearing a WT bone marrow by inoculation of the ICD vaccine (**Fig. 4F**). Both strategies to

systemically augment soluble CALR levels led to an expansion of myeloid-derived suppressor cells (MDSC) in the spleen, as well as in the circulation, supporting the notion that they induce a systemic level of immunosuppression (**Fig. S4A-D**).

In conclusion, artificial supply of soluble CALR as a recombinant protein, as well as provision of a hematopoietic stem cell compartment that releases soluble CALR into the circulation similarly subverted the immune response against cancer cells that succumb to ICD.

Local immunosuppressive activity of soluble CALR. Hydrodynamic injection of vectors coding for ER-localized streptavidin together with the secretory-SBP-GFP (ss-SBP-GFP) (Zhao et al., 2018) led to the expression of both transgenes in the liver with the consequent retention of the GFP fluorescence in hepatocytes, unless mice received intraperitoneal (*i.p.*) injections of biotin (**Fig. 5A-D**). Hence, the RUSH system functions *in vivo*. Next, we examined the possibility that a RUSH-controlled local release of mutant CALR from cancer cells *in vivo* would be sufficient to cause immunosuppression. In a first step, we introduced the RUSH system (without GFP, which is a strong antigen) (Stripecke et al., 1999) into mouse cancer cells. Thus, MCA205 cells were engineered to express ER-retained streptavidin. These cells were then transfected with SBP-wtCALR, SBP-mt1CALR or SBP-mt2CALR (**Fig. 5E**) and formed subcutaneous tumors with undistinguishable growth kinetics in immunocompetent C57Bl/6 mice. Immunofluorescence staining (using an anti-SBP antibody) revealed that the tumors contained equivalent amounts of the SBP-CALR fusion constructs and that systemic (intraperitoneal) injection of biotin provoked the loss of the SBP signal only from SBP-mt1CALR and SBP-mt2CALR cells, but not SBP-wtCALR cells, *in vivo* (**Fig. 5F,G**). Next, we treated mice bearing established SBP-wtCALR,

SBP-mt1CALR or SBP-mt2CALR tumors with the immunogenic chemotherapeutic MTX, either alone or in combination with biotin (**Fig. 5H**). When administered as a standalone treatment, MTX efficiently reduced the growth of all MCA205 tumors, irrespective of their genotype. Biotin did not affect the capacity of MTX to control the growth of untransfected MCA205 cells (**Fig. 5I**) nor that of SBP-wtCALR cells that retain CALR in the ER (**Fig. 5J**). However, biotin interfered with MTX-mediated tumor growth reduction when the tumor expressed biotin-releasable SBP-mt1CALR or SBP-mt2CALR (**Fig. 5K, L**). When MTX was replaced by another ICD inducer, oxaliplatin (OXA), similar results were obtained (**Fig. S5A-D**). Importantly, the *in vitro* cytotoxicity of MTX or OXA was not influenced by the introduction of the RUSH system into cells nor by their treatment with biotin (**Fig. S5E,F**). Altogether, these findings support the idea that soluble CALR released from cancer cells can mediate local immunosuppression, thus interfering with the therapeutic effects of chemotherapeutic ICD inducers.

Immunosuppression by cancer-associated mutations leading to CALR secretion. We next investigated whether 'natural' CALR mutants (without fusion to SBP and without the presence of a streptavidin hook, which both might alter the antigen properties of the cancer cells) would mediate similar effects. For this, we used the CRISPR/Cas9 system to carry out homozygous deletion (Mut1) or insertion (Mut2) that mimic the genetic alterations in the *CALR* gene associated with human myelofibrosis (**Fig. S6A**). Genomic knock-in affected spontaneous tumor growth kinetics yet in contrast to tumors expressing wild type CALR (which is retained in the ER) that responded to immunogenic chemotherapy, tumors arising from clones expressing mt1 or mt2 CALR which are released into the extracellular space (**Fig. S6B**) failed to reduce their growth rate in response to treatment with MTX (**Fig. 6A-F**) or OXA (**Fig. S6C**), but similarly lost their viability in response to MTX or OXA *in vitro* (**Fig. S6D,E**). Surface-bound CALR

serves as a dominant pro-phagocytic signal (the 'eat-me' signal) on cancer cells and is counterbalanced by CD47 (the 'don't-eat-me' signal) (Chao et al., 2010). Thus, CD47 blockade can induce cancer cell phagocytosis depending on CALR surface exposure CALR (Chao et al., 2010; Gardai et al., 2005). While CD47 blockade reduced the growth of control MCA205 fibrosarcomas, it failed to affect the progression of tumors expressing mt1 or mt2 CALR (**Fig. S6F**). Of note, when CALR was released spontaneously from mt1 and mt2 tumor cells *in vivo*, this caused a systemic increase in the frequency of G-MDSC (**Fig. S6G,H**).

More importantly, mutations of CALR could be identified in a sizeable proportion of solid tumors (**Fig. 6G**), and such mutations were significantly ($P<0.04$, chi square test) more frequent in the C-terminal portion of the protein (28 mutations between residues 279 and 416) than in the rest of the protein (35 mutations). We generated mouse tumor cells carrying CALR mutants that lost the ER-retention signal KDEL, either due to the substitution of glutamic acid 405 by a stop codon (E405*) or due to the removal of a splice acceptor site upstream of amino acid 352 (X352) (**Fig. S6A**). These mutations were chosen because of their proximity to the KDEL motif and because they can be considered as representative of solid tumor-associated mutations that, in contrast to MPN-associated CALR mutations, do not generate a frame-shifted new C-terminus. Such CALR mutants caused the spontaneous secretion of CALR protein but not that of other ER-associated proteins such as calnexin (CALN) and protein disulfide isomerase family A member 3 (PDIA3) (**Fig. S6B,I**). When implanted into mice, tumors expressing either E405* or X352 CALR mutants were less responsive to treatment with MTX or OXA (**Fig. 6H-L**) than control tumors. Thus, CALR mutations associated with solid, non-hematopoietic cancers may affect the therapeutic response as well. Of note, in the conditions that we have chosen, the tumor growth-reducing effect of chemotherapy is entirely mediated by a T-lymphocyte-dependent immune

response (**Fig. S7A**,**B)** (Liu et al., 2019; Vacchelli et al., 2015). As previously described (Pietrocola et al., 2016), chemotherapy with MTX improved the CD8/Treg ratio in the immune infiltrate of WT tumors, but failed to do so in tumors expressing mt1CALR, mt2CALR and E405*CALR (**Fig. 7A**). In addition, MTX favored the uptake of tumor cells expressing the pH-resistant ZsGreen fluorescent protein by $CD11C^{+}MHC\text{-}II^{hi}$ $CD80^{hi}$ DC present in the local immune infiltrate only in WT tumors, not in tumors expressing mutant, secretable CALR (**Fig. 7B-D**). Moreover, we concentrated different SBP-CALR mutant proteins, including E405* and X352 that are secreted by the RUSH-CALR cell lines upon biotin induction (**Fig.S7 C**), and found that these mutant proteins inhibited phagocytosis to the same extent as wtCALR when immature DC were confronted with CALR exposing cancer cells (**Fig.S7 D**).

In a final step, we directly compared the response of mice bearing tumors with wild type *Calr* or *Calr* mutations associated with myeloproliferation (mt1 and mt2) or solid cancers (E405* and X352) to PD-1 blockade. Of note, all *CALR* mutations causing the secretion of the protein interfered with tumor growth reduction by immunotherapy to a similar degree. This result was obtained for both MCA205 fibrosarcomas (**Fig. 7E-J**) and TC1 non-small cell lung cancers (**Fig. 7K-P**).

In conclusion, it appears that the secretion of soluble CALR by malignant cells has strong immunosuppressive effects.

Discussion

In the present paper, we used the recently developed RUSH system (Boncompain et al., 2012; Liu et al., 2017; Zhao et al., 2018) to resolve questions on the trafficking of myeloproliferative disease-associated CALR mutants, showing that both CALRdel52 (mt1CALR) and CALRins5 (mt2CALR) undergo conventional protein secretion. In response to biotin added to cultured cells or injected into mice, both CALR mutants carrying SBP in their N-terminus, either alone or fused to GFP, differ in their behavior from wtCALR in the sense that they are released through the Golgi apparatus into the extracellular milieu. These results obtained by the RUSH assay have been validated by experiments involving genetically manipulated cells or mice, in which mtCALR1 and mtCALR2 (as well as additional mutants CALR E405* or CALR X352 but not wtCALR) are released from cells. Moreover, in patients with MPN-associated CALR mutations, plasma CALR and leukocyte-bound CALR were elevated with respect to healthy controls. These results demonstrate the potential utility of this chemical biological system for *in vivo* manipulations that reflect the pathophysiological reality. Indeed, it is conceivable to (in)activate secretory pathways or the subcellular trafficking of receptors by administering biotin or reversible biotin-mimetic molecules at will, in a variety of different applications (Terai et al., 2015). The possibility to switch on or off the system rather rapidly differs from other reversible chemical biological tools such as Tet-on and Tet-off systems that respond with a rather long latency and tend to be 'leaky' (Costello et al., 2018).

Beyond these technological considerations, it appears that MPN-associated CALR mutations are not only oncogenic because they cell-autonomously activate the thrombopoietin receptor but also because they subvert anticancer immunosurveillance. Indeed, our results suggest that CALR

released from cells carrying the CALRdel52 (mt1CALR) and CALRins5 (mt2CALR) mutations can act in an immunosuppressive fashion by inhibiting the recognition and phagocytosis of stressed and dying cancer cells by DC, thus suppressing the antitumor immune response. This has been shown in several systems, *in vitro* and *in vivo* (in mice), using several ways to increase extracellular CALR concentrations, namely (i) by providing an excess of recombinant soluble CALR protein, (ii) by manipulating the hematopoietic system to express mtCALR1, which then becomes detectable in the plasma, and (iii) by implanting tumors that release mt1CALR or mt2CALR (or other solid cancer-associated CALR mutants lacking the C-terminal KDEL motif). Based on the combined results obtained by these experiments, we conclude that extracellular CALR is indeed immunosuppressive. This immunosuppression may also involve shifts in the composition of immune subpopulations (such an increase in MDSC) when CALR becomes elevated at the systemic level, as previously reported (He et al., 2017).

At the conceptual level, the aforementioned results support the general notion that oncogenesis must be facilitated by the simultaneous occurrence of two processes, namely, (i) the activation of cell-autonomous oncogenic drivers (and the inactivation of oncosuppressors) to create malignant cells and (ii) the escape from immunosurveillance by 'hiding' from the immune system or by active immunosuppression. In the case of myeloproliferative diseases, CALR mutations may well fulfill the dual function of (i) providing an autocrine proliferative signal and (ii) subverting the immune response. This important immunosuppressive effect of mutant CALR may explain why CALR mutated MPNs manifest about ten years earlier than JAK2V617F MPNs (Vainchenker and Kralovics, 2017). It should be noted that CALR mutations associated with myeloproliferative diseases are unique in the sense that insertion or deletions in exon 9 of the *CALR* gene create a new C-terminus that facilitates binding to the thrombopoietin receptor, and its activation by

inducing its dimerization through oligomerization of CALR mutants. Thus, beyond the removal of the ER retention signal (KDEL) causing mislocalization of the CALR protein outside of the ER, the specific structure of the new C-terminus contributes to disease pathogenesis. Indeed, single nucleotide mutations that lead to generation of stop codons within exon 9 are unable to activate the thrombopoietin receptor, and such mutations are not observed in myeloproliferative diseases (Elf et al., 2016). Thus, in MPN, the secretion of CALR is not able by itself to induce a disease. In sharp contrast, such stop mutations as well as mutations of the splicing sites ensuring translation of exon 9 occur in a sizeable number of solid cancers (**Data file S1**). It is tempting to speculate that such stop mutations and splice mutations occur because carcinoma and sarcoma cells usually do not express the thrombopoietin receptor (and hence do not positively select for specific deletion and insertion mutations creating new C-termini), yet still might cause immunosuppression due to the release of soluble CALR from the cells. Probably, such solid-tumor associated *CALR* mutations do not function as oncogenic drivers (as this is the case in MPN), but rather play a subordinate role contributing to local immunosuppression.

Of note, several prominent autoimmune diseases are characterized by anti-CALR auto-antibodies. This applies to primary biliary cirrhosis, rheumatoid arthritis and systemic lupus erythematosus (Wiersma et al., 2015). It can be speculated, yet remains to be demonstrated, that such auto-antibodies might quench extracellular CALR, which indeed can be measured at background levels in the plasma of mice and healthy human individuals. If the baseline levels of CALR had a homeostatic immunosuppressive function, their quenching by autoantibodies might favor autoimmune and inflammatory reactions. Beyond this conjecture, which requires in-depth exploration, the work presented here argues in favor of an immunosuppressive role of excessive levels of extracellular CALR protein released from neoplastic cells bearing *CALR* mutations.

Acknowledgments: GK and LZ are supported by the Ligue contre le Cancer (équipe labellisée); Agence National de la Recherche (ANR) – Projets blancs; ANR under the frame of E-Rare-2, the ERA-Net for Research on Rare Diseases; Association pour la recherche sur le cancer (ARC); Cancéropôle Ile-de-France; Chancelerie des universités de Paris (Legs Poix), Fondation pour la Recherche Médicale (FRM); a donation by Elior; European Research Area Network on Cardiovascular Diseases (ERA-CVD, MINOTAUR); Gustave Roussy Odyssea, the European Union Horizon 2020 Project Oncobiome; Fondation Carrefour; High-end Foreign Expert Program in China (GDW20171100085 and GDW20181100051), Institut National du Cancer (INCa); Inserm (HTE); Institut Universitaire de France; LeDucq Foundation; the LabEx Immuno-Oncology; the RHU Torino Lumière; the Seerave Foundation; the SIRIC Stratified Oncology Cell DNA Repair and Tumor Immune Elimination (SOCRATE); and the SIRIC Cancer Research and Personalized Medicine (CARPEM). IP, CM and WV were funded by INCA PLBio 2015 and by the Ligue contre le Cancer (équipe labellisée). FP is supported by the ANR, the Institut Curie, the Centre National de la Recherche Scientifique (CNRS).

Author contributions: P.L, L.Z, F.L, C.M, W.X, I.M, S.L, and B.Q performed most of the experiments; E.W and P.E produced and provided the recombinant calreticulin; D.R and C.L performed the bioinformatics summarization of the *CALR* mutation information; O.K, L.Z and G.K conceived the study; I.P, W.V, F.P, C.L, and P.E designed (parts of) the study; P.L, L.Z, O.K and G.K wrote the paper.

Conflict of interest disclosure: The authors declare no conflict of interest.

Figure legends

Figure 1. Detection of mt1CALR and mt2CALR release via the RUSH assay.

A-F. Comparison of GFP, wild type and mutant calreticulin with respect to their secretory capacity in the RUSH assay. In the absence of biotin (black circles), U2OS cells stably co-expressing streptavidin (Str)-KDEL and different fusion proteins containing combinations of streptavidin binding protein (SBP), green fluorescent protein (GFP) and/or wild type or mutant calreticulin (CALR) retained these reporters in the ER as depicted in the scheme (**A**). Two hours after the addition of biotin at a final concentration of 40 µM, the SBP-GFP control was released from the ER (**B**). Wild type (wt) reporter SBP-GFP-wtCALR remained in the ER (**C**), while the mutant (mt) reporters SBP-GFP-mt1CALR or SBP-GFP-mt2CALR was released from the ER and secreted by the cell (**D,E**). Quantitative results (means ± SD, three experiments) are reported as the cytoplasmic GFP intensity normalized to untreated cells (**F**). Asterisks indicate significant effects (***$p < 0.001$, Student t test comparing results with and without (w/o) biotin). **G-I**. Effects of brefeldin A on the secretion of mutated CALR. In the absence of brefeldin A (BFA), SBP-GFP-mtCALR reporters transported from the ER to the Golgi upon biotin addition, accumulated on the Golgi at 30 min post biotin addition, and secreted from cells after 2 hours. Pretreatment of the RUSH cells with BFA disrupted the Golgi (**H,I**) and inhibited the release process. Golgi membrane was labeled with a B4GALT1 antibody. The colocalization of GFP and GALT1 is quantified before, 30 and 120 min after addition of biotin in cells that were pretreated or not with BFA (**J**; means ± SD, $n = 3$). Asterisks indicate significant effects (***$p < 0.001$, Student *t* test comparing with results without biotin (0')). Scale bars equal 10 µm.

Figure 2. Detection of mtCALR release in cell culture supernatants and patients' plasma/PBMC.

A-E, U2OS cells stably co-expressing streptavidin (Str)-KDEL hook and streptavidin binding protein–green fluorescent protein-calreticulin (SBP-GFP-CALR) wild type (wt) or mutant (mt) reporters were left untreated or were pretreated with 10 µg/mL brefeldin A (BFA) for 2 h. To precipitate supernatant protein and extract intracellular protein for immunoblot, cells were further incubated with biotin for additional 4 hours (**A,B**). SBP-GFP-CALR reporters were detected by anti-SBP and anti-GFP antibodies. Beta-actin was assessed as loading control. Alternatively, cells were incubated with biotin for different periods after BFA pretreatment and supernatant was collected for sandwich ELISA (**C-E**). Whole lysis of the same amounts of cells in equivalent volumes of medium for each cell line was used as standards (100%) and the spontaneous or biotin-induced release of CALR into supernatants refers to these standards. Data are shown as means ± SEM (n = 3; *p < 0.05, **p < 0.01, and ***p < 0.001, two-tailed Student's t test, compared to biotin$^-$/BFA$^-$control condition). **F**, the concentration of circulating CALR in the plasma of patients with myeloproliferative neoplasms (MPN) carrying mt1CALR or mt2CALR, as well as that of healthy volunteers (WT), was measured by means of ELISA. Data are shown as scatter dot plot. *p < 0.05; ****p < 0.0001 (two-tailed Student's t test) as compared with data from plasma of healthy volunteers**. G,H,** Peripheral blood mononuclear cells (PBMCs) from healthy volunteers or MPNs patients with CALR mutations were subjected to immunostaining of surface CALR and detected by means of flow cytometry analysis. CALR median fluorescence intensity of monocytes (**G**) and lymphocytes (**H**) were analyzed and data are shown as scatter dot plot. *p < 0.05 (two-tailed Student's t test,) as compared with data from healthy volunteers**.**

Figure 3. Soluble recombinant CALR interferes DC mediated phagocytosis.

MCA205 cells pre-labeled with CellTracker orange CMTMR dye were either or not (Ctr) treated with oxaliplatin (OXA) for 24 h, while bone marrow-derived dendritic cells (BMDCs) were incubated with different amounts of recombinant CALR (rCALR) protein (2.5, 5, 10 or 20 µg per million cells), alone or in combination with polymyxin B, for 30 min at room temperature. BMDCs and MCA205 cells (1:4) were co-cultured at 37° or 4° C for 6 hours for the staining of mouse CD11c_ AlexaFluor488 antibody. Phagocytosis was assessed by both regular flowcytometric (Fortessa) and imaging-cytometric (Amnis) analysis of double positive cells. Representative dot plots (**A**) and Amnis-captured images (**C**), as well as the quantification of double positive events (means± SD, $n = 3$) (**B,D,E**) are reported. Scale bars equal to 10 µm. Statistical significance was calculated by means of two-tailed Student's t test, $^{***}p < 0.001$ as compared to Ctr, $^{###}p < 0.001$ as compared to MCA OXA plus BMDC no rCALR. **(F)**, Scheme of the *in vivo* phagocytosis assay. MCA205 cells pre-labeled with PKH26 dye were either or not (Ctr) treated with oxaliplatin (OXA) for 24 h. Naïve mice received an intravenous (*i.v.*) injection of rCALR or equivalent PBS, while the mice carrying the type I CALR mutation ($CALR_{del52}$) received only PBS, one hour before the intrasplenic injection of MCA205 cells. Blood and spleens were collected three hours later. Plasma CALR concentration was measured by means of ELISA (**G**), and splenocytes were subjected to immunostaining of CD11c antibody to assess phagocytosis (**H-J**). Representative histograms of flow cytometric analyses are shown in (**H,I**). The phagocytotic events are quantified as the percentage of double positive events (**J**). Statistical significance was calculated by ANOVA test for multiple comparison, $^{**}p < 0.01$, $^{****}p < 0.0001$ as compared with data from *i.v.* PBS/ MCA205 controls; $^{####}p < 0.0001$ as compared with data from *i.v.* PBS/MCA205 OXA.

Figure 4. Saturated soluble CALR interferes with vaccination efficacy of dying cancer cells.

MCA205 cells were pretreated by mitoxantrone (MTX) for 24 hours before subcutaneously (*s.c.*) injected to naïve C57Bl/6 mice (**A-C**), or mice transplanted with bone marrow (BM) from wild type mice (WT) or calreticulin del52 mutation bearing mice ($CALR_{del52}$) (**D-F**), as a vaccination. When applicable naïve mice received an intravenous (*i.v.*) injection of recombinant CALR ($rCALR_{i.v.}$+) or equivalent PBS ($rCALR_{i.v.}$-) together with the vaccine and reinforced 12 h later (**A**). Blood were collected one hour after the second *i.v.* injection, and plasma CALR concentration was measured by means of ELISA (**B,E**). All mice were rechallenged with live MCA205 cells after one week. Tumor incidence was recorded and reported as Kaplan–Meier curves (**C,F**). Statistical significance was calculated by means of the Likelihood ratio test. $^{***}p < 0.001$ compared to PBS group, $^{\#\#\#}p < 0.001$ as comparing indicated groups (n = minimum 7 animals per group).

Figure 5. Inducible mtCALR release by means of the *in vivo* RUSH assay.

Vectors encoding the KDEL-streptavidin (Str) hook and the secretory reporter ss-SBP-GFP were co-expressed in hepatocytes by hydrodynamic tail vein injection before intraperitoneal (*i.p.*) injection of biotin (**A**). Livers were subjected to confocal immunofluorescence using an Alexa Fluor 647-Str antibody, Alexa Fluor 568-phalloidin and DAPI, scale bars equal 10 μm (**B**). Quantification of cytoplasmic GFP (CytoGFP) intensity (**C**) and Str intensity (**D**) in Str positive hepatocytes (**C**). Each dot represents a random view (3 mice, 10 views each) acquired by confocal microscopy, $^{****}p < 0.0001$ (two-tailed Student's t test,). (**E-L**) MCA205 cells stably co-expressing KDEL-Str with streptavidin-binding peptide-calreticulin (SBP-CALR) wild type (wt), mutation type I (mt1), or type II (mt2) reporters were subcutaneously (*s.c.*) inoculated to C57Bl/6 mice to establish the *in vivo* RUSH model. To validate the inducible mtCALR release, the RUSH-bearing mice received an intraperitoneal (*i.p.*) biotin injection and tumors were

harvested 4 or 8 hours later for immunostaining with the anti-SBP antibody (**E**). Representative confocal images are displayed in (**F**), scale bars equal 10 µm; quantification of cytoplasmic SBP-fluorescence (CytoFluor) intensity is displayed as box plots with individual points (**G**, each point represents a random view). ****$p < 0.0001$ compared to the 0 h measurement (*t* test). (**H**) RUSH-bearing mice were treated with *i.p.* mitoxantrone (MTX) or equivalent PBS at day 0 and day 2, accompanied by daily *i.p.* administration of biotin. Tumor development was monitored and the tumor growth curves were subjected to type II ANOVA test for pairwise comparisons across groups (**I-L**). ***$p < 0.001$ compared to Ctr group (PBS without biotin), $^{###}p < 0.001$ as compared to biotin + MTX group ($n = 6$ animals per group).

Figure 6. Genome engineering mediated CALR mutations desensitize solid tumors to immunogenic chemotherapy.

Calreticulin (CALR) mutant (mt) MCA205 clones as well as wild type (wt) MCA205 cells were subcutaneously (*s.c.*) inoculated to C57Bl/6 mice to establish different cancer models, which were treated with mitoxantrone (MTX) or oxaliplatin (OXA) as described in panel (**A**). (**B-F**) Developments of MCA205 tumors carrying the CALR type I and type II mutations (mt1/mt2) were reported (2 clones for each mutation) and the tumor growth curves were subjected to type II ANOVA test for pairwise comparisons across groups. ***$p < 0.001$ compared to PBS group (Ctrl), (*n.s.* means not significant, $n = 6$ animals per group). Distribution of CALR mutations associated to myeloproliferative neoplasms, as annotated in COSMIC, as well as that to solid tumors as annotated in COSMIC and cBioPortal, are summarized in (**G**). In solid tumors, mutations are significantly ($p < 0.04$, Xi square test) more frequent in the C-terminal portion of the protein (28 mutations between residues 279 and 416) than in the rest of the protein (35 mutations). Mutations within the C-terminal domain that affect the KDEL motif, Stop codons,

frameshift mutation and splicing mutations are annotated in blue or red. Other mutations of this type close to the C-terminus are labelled in green (**H-L**) Progression of MCA205 tumors carrying the glutamic acid 405 to stop codon mutation (E405*) or a splice (X352) mutation, that were treated with MTX or OXA. Tumor growth curves were subjected to type II ANOVA test for pairwise comparisons across groups. $^{**}p < 0.01$; $^{****}p < 0.0001$ compared to PBS group (Ctrl). $n = 6$ animals per group.

Figure 7. *Calr* mutations in cancer cells change immune infiltration and subvert immunotherapy.

(**A-D**) ZsGreen expressing MCA205 (*Calr* wt or mutant) tumor-bearing mice were treated with mitoxantrone (MTX) or equivalent PBS at day 0 and day 2 since tumors became palpable. Tumors were collected at day 10 and digested to generate viable single cells for the cytofluorimetric analysis of T cell markers or dendritic cell (DC) markers ($n = 10$ animals/group). Frequency of $CD8^+$ T cells and regulatory T cells (Tregs, defined as $CD4^+CD25^+FOXP3^+$ cells) was quantified as percentage among $CD3^+$ cells, and the ration of $CD8^+$ over Tregs is shown in (**A**). DCs are defined as $CD45^+CD11C^+CD80^{hi}MHC\text{-}II^{hi}$, and $ZsGreen^+$ cells were gated from this population to show the uptake of tumor cells by DCs. Representative plots showing the increase in the ZsGreen signal among DCs infiltrating wt tumors (**B**) and CALR mt2 tumors (**C**). Percentages of $ZsGreen^+$ DCs are summarized as box plots (**D**). Statistical significance was calculated by means of the ANOVA test, $^{***}p < 0.001$ as comparing between indicated groups. MCA205 (**E-J**) or TC-1 (**K-P**) cells, which were either wt or subjected to the indicated CALR mutations (mt1, mt2, E405* or X352), were implanted in C57BL/6 mice. Once the tumors became palpable, mice were treated by systemic (*i.p.*) injections of a PD-1 blocking antibody (or an isotype control antibody), and this treatment was repeated 4 and 8 days later. The difference

(Δ) of tumor growth for groups treated with PD-1-specific and isotype control antibodies was computed for comparison across genotypes (**J** and **P**). Tumor growth curves were subjected to type II ANOVA test for comparisons (nominal p-values indicated for comparisons between isotype controls and PD-1 antibody-injected mice) and across groups (*$p < 0.05$; **$p < 0.01$; ***$p < 0.001$; ****$p < 0.0001$ compared to the wt; $n = 5$ animals per group).

STAR* Methods

KEY RESOURCES TABLE

REAGENT or RESOURCE	SOURCE	IDENTIFIER
Antibodies		
Mouse monoclonal anti-streptavidin	Santa Cruz Biotechnology	sc-52234
Mouse monoclonal anti-SBP	Santa Cruz Biotechnology	sc-101595
Rabbit polyclonal anti-calreticulin	Abcam	ab02873
Rabbit polyclonal anti-GFP	Abcam	ab6556
Rabbit polyclonal anti-GBF1	Abcam	ab86071
Rabbit polyclonal anti-GM130	Abcam	ab52649
Mouse monoclonal anti-β-actin (HRP)	Abcam	ab49900
Rabbit polyclonal anti-B4GALT1	Abnova	PAB20512
Rabbit polyclonal anti-ERp57	Invitrogen	PA529810
Rabbit polyclonal anti-Calnexin	Invitrogen	PA534754
Chicken polyclonal anti-calreticulin	Invitrogen	PA1-902
Alexa Fluor® 488-conjugated anti-mouse CD11c	Biolegend	117311
Purified anti-mouse CD16/CD32	Biolegend	101302
Pacific Blue-conjugated anti-mouse CD11b	eBioscience	RM2828
Alexa Fluor® 488-conjugated anti-mouse Ly-6C	eBioscience	53-5932-82
PE-conjugated anti-mouse Ly-6G	eBioscience	12-9668-82
APC_eFluor780-conjugated anti-mouse CD45	eBioscience	47-0451-82
PerCP_Cy5.5-conjugated anti-mouse CD80	Biolegend	104722
APC-conjugated anti-mouse MHC II	Biolegend	107614
PE_Cy7-conjugated anti-mouse CD11c	Biolegend	117318
APC-conjugated anti-mouse CD3	Biolegend	100236
eFluor450-conjugated anti-mouse CD4	eBioscience	48-0042-82

Alexa Fluor® 594-conjugated anti-mouse CD8a	Biolegend	100758
PE_Vio770-conjugated anti-mouse CD25	Miltenyi	130-123-893
FITC-conjugated anti-mouse FOXP3	eBioscience	11-5773-82
Rat monoclonal anti-CD47	BioXcell	BE0270
Rat monoclonal isotype antibody	BioXcell	BE0089
Rat monoclonal anti-PD-1	BioXcell	BE0273
Rat monoclonal isotype antibody	BioXcell	BE0090
Rat monoclonal anti-CD4	BioXcell	BE0003-1
Rat monoclonal anti-CD8	BioXcell	BE0061
Bacterial and Virus Strains		
pCDH-Streptavidin-KDEL	Boncompain et al., 2012	Addgene 65307
pCDH-ss-SBP-EGFP	Zhao et al., 2019	DOI: 10.1038/s41598-018-33378-y.
pCDH-SBP-EGFP-wtCALR	This paper	N/A
pCDH-SBP-EGFP-mt1CALR	This paper	N/A
pCDH-SBP-EGFP-mt2CALR	This paper	N/A
pCDH-SBP-wtCALR	This paper	N/A
pCDH-SBP-mt1CALR	This paper	N/A
pCDH-SBP-mt2CALR	This paper	N/A
pCDH-SBP-CALR$_{delKDEL}$	This paper	N/A
pCDH-SBP-CALRE$_{405*}$	This paper	N/A
pCDH-SBP-CALRE$_{x352}$	This paper	N/A
pX458	Ran et al., 2013	Addgene 48138
pLC-ZsGreen-P2A-Blast	Patil et al., 2018	Addgene 123322
pLC-ZsGreen-Blast	This paper	N/A
pDisplay™ Mammalian Expression Vector	Thermo Fisher	V66020

Biological Samples		
Healthy adult plasma	Gustave Roussy Cancer Center	N/A
Healthy adult PBMCs	Gustave Roussy Cancer Center	N/A
Plasma of myeloproliferative neoplasms patients	Gustave Roussy Cancer Center	N/A
PBMCs of myeloproliferative neoplasms patients	Gustave Roussy Cancer Center	N/A
Chemicals, Peptides, and Recombinant Proteins		
Biotin	Sigma	B4501
Avidin from egg white	Sigma	A9275
Brefeldin A	Sigma	B5936
Geneticin	Thermo Fisher	10131027
Hygromycin B	Thermo Fisher	10687010
Blasticidin	InvivoGen	ant-bl-10p
Mitoxantrone	Sigma	M2305000
Oxaliplatin	Sigma	Y0000271
Polymyxin B sulfate salt	Sigma	P4932-5MU
Ponceau S solution	Sigma	P7170-1L
Hoechst 33342	Thermo Fisher	H3570
Recombinant mouse GM-CSF	PeproTECH	315-03
DAPI	Thermo Fisher	62248
Propidium Iodide	Thermo Fisher	P3566
Recombinant CALR protein	Culina et al., 2004	DOI:10.1074/jbc.M410841200

Critical Commercial Assays		
Human calreticulin ELISA kit	RayBiotech	ELH-CALR-1
ViraPower™ lentiviral packaging mix	Thermo Fisher	K497500
Phusion® High-Fidelity PCR Master Mix	New England BioLabs	M0531
Monarch® DNA Gel Extraction Kit	New England BioLabs	T1020
ECL Prime Western Blotting Detection Reagent	GE Healthcare	RPN2232
Pierce® Protein A Agarose beads	Thermo Fisher	20333
1-Step™ Ultra TMB-ELISA substrate	Thermo Fisher	34028
CellTracker orange CMTMR dye	Thermo Fisher	C2927
PKH26 Red Fluorescent Cell Linker	Sigma	PKH26GL-1KT
Ficoll Paque Plus	GE Healthcare	17-1440-02
pHrodo™ Green BioParticles	Thermo Fisher	P35366
Pierce LAL Chromogenic Endotoxin Quantitation Kit	Thermo Fisher	88282
eBioscience™ Foxp3 / Transcription Factor Staining Buffer Set	Thermo Fisher	00-5523-00
DC™ Protein Assay	Bio-Rad	5000111
QuikChange Lightning Site-Directed Mutagenesis Kit	Agilent Technologies	210519
Deposited Data		
Experimental Models: Cell Lines		
Human osteosarcoma U2OS	ATCC	HTB-96
Human cervix adenosarcoma HeLa	ATCC	CCL-2
Mouse fibrosarcoma MCA205	Merck	SCC173
Engineered human embryonal kidney cell 293FT	Invitrogen	R70007

U2OS-Str-KDEL/ss-SBP-EGFP	Zhao et al., 2018	DOI: 10.1038/s41598-018-33378-y
U2OS-Str-KDEL/SBP-EGFP-wtCALR	This paper	N/A
U2OS-Str-KDEL/SBP-EGFP-mt1CALR	This paper	N/A
U2OS-Str-KDEL/SBP-EGFP-mt2CALR	This paper	N/A
HeLa-Str-KDEL/SBP-EGFP-wtCALR	This paper	N/A
HeLa-Str-KDEL/SBP-EGFP-mt1CALR	This paper	N/A
HeLa-Str-KDEL/SBP-EGFP-mt2CALR	This paper	N/A
MCA205 CALR Del52	This paper	N/A
MCA205 CALR Ins5	This paper	N/A
MCA205 CALR E405*	This paper	N/A
MCA205 CALR X352	This paper	N/A
MCA205-Str-KDEL/SBP-wtCALR	This paper	N/A
MCA205-Str-KDEL/SBP-mt1CALR	This paper	N/A
MCA205-Str-KDEL/SBP-mt2CALR	This paper	N/A
MCA205-Str-KDEL/SBP-CALR$_{delKDEL}$	This paper	N/A
MCA205-Str-KDEL/SBP- CALR$_{E405*}$	This paper	N/A
MCA205-Str-KDEL/SBP- CALR$_{X352}$	This paper	N/A
MCA205 CALR Del52-ZsGreen	This paper	N/A
MCA205 CALR Ins5-ZsGreen	This paper	N/A
MCA205 CALR E405*-ZsGreen	This paper	N/A
MCA205 CALR X352-ZsGreen	This paper	N/A
MCA205-ZsGreen	This paper	N/A
MCA205-pDisplay^{TM}-CALR	This paper	N/A
Experimental Models: Organisms/Strains		
Mouse C57Bl/6	ENVIGO France	REF KA02
Mouse C57Bl/6 CALRdel52	Marty et al, 2016	DOI: 10.1182/blood-

		2015-11-679571
Mouse C57Bl/6 CALRwt	Marty et al, 2016	DOI: 10.1182/blood-2015-11-679571
Oligonucleotides		
gRNA coding sequence for CALR mutation Del52 and X352	This paper	See the Supplementary Table 1.
gRNA coding sequence for CALR mutation Ins5 and E405*	This paper	See the Supplementary Table 1.
Forward PCR primer for amplifying CALR mutation containing regions	This paper	See the Supplementary Table 1.
Reverse PCR primer for amplifying CALR mutation containing regions	This paper	See the Supplementary Table 1.
Sequence primer for the CALR mutation containing regions	This paper	See the Supplementary Table 1.
QuickChange Lightening primers to delete the KDEL motif in pCDH-SBP-wtCALR plasmid	This paper	See the Supplementary Table 1.
QuickChange Lightening primers to induce the E405* mutation in pCDH-SBP-wtCALR plasmid	This paper	See the Supplementary Table 1.
QuickChange Lightening primers to induce the X352 mutation (deletion of A352-L417) in pCDH-SBP-wtCALR plasmid	This paper	See the Supplementary Table 1.
QuickChange Lightening primers to remove the P2A tag from pLC-ZsGreen-P2A-blast plasmid	This paper	See the Supplementary Table 1.
Recombinant DNA		
Homology template for inducing CALR mutation	This paper	See the

Del52		Supplementary Table 1.
Homology template for inducing CALR mutation Ins5	This paper	See the Supplementary Table 1.
Homology template for inducing CALR mutation E405*	This paper	See the Supplementary Table 1.
Homology template for inducing CALR mutation X352	This paper	See the Supplementary Table 1.
Software and Algorithms		
BD FACSDiva™ Software v8.0	BD Bioscience	https://www.bdbiosciences.com/in/instruments/software/facsdiva/features/overview.jsp
FlowJo VX	FlowJo, LLC	https://www.flowjo.com
Microsoft Office 2016	Microsoft	https://www.microsoft.com/fr-fr/
R Studio	RStudio	https://www.rstudio.com
GraphPad Prism 7	GraphPad Software	https://www.graphpad.com
MetaXpress V5	Molecular Device	https://www.moleculardevices.com/
MetaXpress custom model editor	Molecular Device	https://www.moleculardevices.com/
ImageJ FIJI	NIH	https://imagej.nih.gov/ij/download.html

Wave XFe Desktop V2	Seahorse Bioscience	https://www.agilent.com/en-us/products/cell-
R software	The R Foundation	https://cran.r-project.org/mirrors.html
Chi-Square calculator	Social Science Statistics	http://www.socscistatistics.com/tests/chisquare/Default2.aspx
Leica LAS X software	Leica Biosystems	http://www2.leicabiosystems.com/l/48532/2014-11-18/35cqc
ImageQuant LAS4000	GE Healthcare	https://www.gelifesciences.com/ko/kr/shop/molecular-biology/nucleic-acid-electrophoresis--blotting--and-detection/molecular-imaging-for-nucleic-acids/imagequant-las-4000-series-p-00039
GPP Web Portal	Broad Institute	https://portals.broadinstitute.org/gpp/public/analysis-tools/sgrna-design

LEAD CONTACT AND MATERIALS AVAILABILITY

Further information and requests for resources and reagents should be directed to and will be fulfilled by the Lead Contact, Guido Kroemer (kroemer@orange.fr).

All unique/stable reagents generated in this study are available from the Lead Contact with a completed Materials Transfer Agreement.

EXPERIMENTAL MODEL AND SUBJECT DETAILS

Cell lines

Wild type human osteosarcoma U2OS, human cervix adenocarcinoma HeLa cells and murine fibrosarcoma MCA205 cells were initially purchased from ATCC (https://www.atcc.org/), and those cells, as well as their derivatives, were cultured in Dulbecco's Modified Eagle Medium (DMEM), supplemented with fetal bovine serum (FBS) (10 %), penicillin (100 U/mL), and streptomycin (100 µg/mL) in a 37°C humidified atmosphere containing 5% CO_2. Engineered RUSH cell lines were always maintained in complete growth media supplemented with G418 and Hygromycin B (Invitrogen, Carlsbad, CA, USA) Cell culture media and supplements were obtained from Gibco Invitrogen and plastic material came from Corning (Corning, NY, USA).

Virus

Lentivirus expressing the pCHD-Str-KDEL hook as well as pCDH-SBP-(GFP)-CALR reporters were produced in 293FT cells by means of the ViraPower™ Lentiviral Expression System from Invitrogen following the manufacturer's protocol. After an overnight incubation at 37°C in a humidified 5% incubator, the medium was replaced with fresh complete growth medium and cells were continuously incubated for additional 48 hours before virus-containing supernatants were harvested and passed through a Millex-HV 0.45 µm PVDF filter (Merk Millipore). The viral supernatants were then directly used for infection of acceptor cells or stored at –80°C for future usage.

Mice

Ethics Statement. All animal experiments were approved by the local Ethics Committee (CEEA IRCIV / IGR n°26, registered with the French Ministry of Research, project number 2016-104), and were in compliance with the 63/2010/EU directive from the European Parliament. C57BL/6 mice (Envigo, Cambridgeshire, UK) were housed in a 12 h light/dark cycles, temperature-controlled environment and received food and water *ad libitum*. Heterozygous or homozygous conditional knock in C57Bl/6 mice bearing humanized C-terminal mutated murine Calr (Calr*del52)* were generated by Cre-Lox recombination strategy and the mutation was expressed by crossing the mice with VavCre transgenic mice. For bone marrow transplantation $3x10^6$ cells were engrafted into lethally irradiated (9.5 Gy) congenic recipient mice. with bone marrow cells transduced with retroviruses expressing this mutant, as described in previous publication (Marty et al., 2016).

Isolation of bone marrow-derived dendritic cells (BMDCs). To obtain myeloid DCs, 6-week-old C57B/l6 animals were euthanized and adequately sterilized before tibiae and femora were extracted and bone marrow (BM) was flushed out with extraction buffer (2% FBS in PBS). After centrifugation at 500 g for 10 min at 4°C, BM cells were resuspended in red cell lysis buffer (0.01M Tris, 0.83% NH_4Cl in Milli-Q water) for 2 min before the immediate addition of 10-fold the volume of DC medium (RPMI 1640 medium supplemented with 10% FBS, 100 U/mL penicillin, 100 µg/mL streptomycin, 1 M HEPES, 1X MEM Non-Essential Amino Acids Solution, 50 µM 2-Mercaptoethanol). The cell suspension was passed through a 70 µm cell strainer before the centrifugation at 500 g for 10 min at 4°C. BM cells were resuspended in DC medium and counted. The cell density was adjusted to one million cells per mL, and the medium was supplemented with 40 ng/mL recombinant mouse GM-CSF. 1 mL of fresh DC medium containing 40 ng/mL of GM-CSF was added at day 3 to reconstitute the medium; 1 mL of supernatant was carefully removed and replaced with fresh DC medium containing 40 ng/mL of

GM-CSF at day 6 to reconstitute again. At day 7, the non-adherent and loosely adherent BMDCs were harvested for further experiments.

In vitro **phagocytosis experiments using BMDC.** MCA205 cells were pre-labeled with 0.4 μM CellTracker orange CMTMR dye (Thermo Fisher Scientific) and then incubated with or without 300 μM oxaliplatin for 24 h before harvest. BMDCs (1×10^6/mL) were pre-coated with the indicated concentrations of recombinant CALR (rCALR) protein, alone or in combination with 2,000 units of polymyxin B (PMB), for 30 min at room temperature before the phagocytosis assay or the surface staining of CALR. CALR produced in a baculovirus system (Obeid et al., 2007) contained low levels of LPS (approximately 0.033 EU, Pierce LAL Chromogenic Endotoxin Quantitation Kit), less than the FDA requires for injectable solutions. BMDCs and MCA205 cells were mixed at a ratio of 1:4 and co-cultured either at 37 °C or 4 °C for 6 h. Cells were harvested and centrifuged at 500g for 10 min, washed with cold PBS and resuspended in Alexa Fluor® 488 anti-mouse CD11c antibody diluted 1/100 in PBS containing 0.5% FBS and 2% BSA. After incubating at 4 °C in the dark for 1 h, the cells were washed with PBS and fixed in 4 % PFA/PBS containing 3 % of sucrose and 2 μg/mL Hoechst 33342. Finally, cells were washed and prepared for common flow cytometry (BD LSRFortessa, BD Biosciences) or imaging flow cytometry (ImageStream® X, Merk Millipore). Double positive cells were counted as phagocytic events.

In vitro **phagocytosis experiments using peritoneal macrophages.** To isolate macrophages from the abdominal cavity, 10 ml of RPMI 1640 medium was injected into the peritoneal cavity with a 25 G needle and the peritoneal fluid was recovered after a short period (~30 seconds) abdomen massage. Peritoneal cells were then spun for 5 min at 300 x g (4 °C) to collect the pellet, which was counted of cell density and adjusted to 1 x 10^6/mL in RPMI medium containing 10% heat-inactivated FBS. Subsequently the peritoneal cells were seeded in 96-well imaging

plates and cultured at 37 °C with 5% CO2 for 3 h. Next, non-adherent cells were removed by extensive washing with RPMI containing 10% heat-inactivated FBS. Adherent cells (macrophages) were stained with 1 µM CellTracker Orange CMTMR dye in serum-free medium containing rCALR 0, 1, 2.5, 5, 10, 20 µg/mL (100 µL for 10^5 cells equal to 1, 2.5, 5, 10, 20 µg/1x10^6 macrophages) for 30 minutes at 37°C. After an additional wash with RPMI containing 10% FBS, 100 µL pHrodo Green particles solution was added per well and the plate was further incubated at 37°C (without CO2) for 2 hours to allow phagocytosis and acidification to reach its maximum. The assayed plates were then scanned and green fluorescence signal was quantified as described above.

In vivo **phagocytosis assay.** MCA205 cells were pretreated or not with 300 µM oxaliplatin for 24 h before being harvested, stained with 5 µM PKH26 dye (Sigma) following the manufacture's protocol, and adjusted to 2 X 10^8 cells\mL in PBS. Under general anesthesia with 4% isoflurane and maintained in a prone position, wild type C57Bl/6 mice (8 weeks), or $CALR_{del52}$ mice (16 weeks) were shaved at the surgical area to avoid contamination, and sterilized with 75% ethanol and iodine of the left subcostal area of the incision. A lateral incision was made on each mouse and an intrasplenic injection of 50 µL PKH26-labelled tumor cells (1x10^7) was performed using a 0.3 mL insulin syringe with 30 G hypodermic needles. Skin incision was closed with a surgical skin clip. If applicable, WT mice received an *i.v.* injection of 200 µg recombinant CALR proteins one hour before the intrasplenic injection of tumor cells. Two hours after the intrasplenic injection, mice were sacrificed, blood was collected to prepare plasma for ELISA measurement of CALR levels with a human CALR ELISA kits (RayBiotech, Norcross, GA, USA) following the manufacture's protocol, and spleens was removed for dissociation with collagenase H (Invitrogen). Cells were filtered through a 70 µm ell strainer, resuspended in red blood cell lysis

buffer, and washed. In the next step, splenocytes were stained with Alexa Fluor® 488 anti-mouse CD11c antibody and phagocytosis was assessed by flow cytometric analysis of double positive cells.

Antitumor vaccination experiments. MCA205 cells were treated with MTX (4 μM) for 24 h in 175 cm^2 flasks before cells were collected and adjusted to a density of $1x10^7$ cells/mL in PBS. Then 100 μL cell suspension was subcutaneously injected into the left flank of wild type C57Bl/6 mice (8 weeks); or $CALR_{del52}$ mice (16 weeks). In parallel, 100 μL PBS was injected in the control group. When applicable, WT mice received 200 μg recombinant CALR protein *i.v.* 1 hour before and 12 hours after the vaccination. Blood was collected one hour after the last injection to prepare plasma for the measurement of CALR by ELISA. One week later, the absence of tumors on the vaccination flank was confirmed and $1x10^5$ living MCA205 cells were injected in the right flank of the animals. Tumor incidence was regularly monitored for the following days and the absence of tumors was considered as an indication of efficient antitumor vaccination.

Chemotherapeutics/Immunotherapeutic assay with established tumor models. MCA205 cells or their derivates containing the designed CALR mutants ($5x10^5$ in 100 μL PBS) were subcutaneously inoculated into the right flank of wild type C57BL/6 mice. When the tumor became palpable (and the surface calculated as longest dimension × perpendicular dimension × π/4 reached around 30 mm^2), mice received *i.p.* 2.6 mg/kg MTX in 200 μL PBS, 10 mg/kg OXA in 200 μL PBS or only 200 μL PBS. Two days later the treatment was repeated. For the treatment with CD47 blockade, animals received *i.p.* 20 mg/Kg anti-CD47 monoclonal antibody (BioXcell, BE0270) or equivalent isotype control antibody (BioXcell, BE0089) daily until the end of the experiment. For the treatment with PD-1 blockade, animals received *i.p.* 10 mg/Kg anti-PD-1 monoclonal antibody (BioXcell, BE0273) or equivalent isotype control antibody (BioXcell,

BE0089), at day0, day4, and day8. For the depletion of T cells, mice received an *i.p.* injection of 100 µg anti-CD8 (clone 2.43 BioXCell) plus 100 µg anti-CD4 (clone GK1.5 BioXCell) at day -1 and day 0. Following the antibodies were supplied once a week for two weeks. Tumor surface was monitored regularly and animals bearing neoplastic lesions that exceeded 250 mm^2 were euthanized.

***In vivo* RUSH assay in established tumors.** As described above, MCA205 cells co-expressing KDEL-Str with SBP-wtCALR, mt1CALR, or mt2CALR were inoculated to the right flank of WT C57Bl/6 mice (8 x 10^5/mouse in 100 µL PBS), naïve MCA205 cells were used as control. When tumors became palpable (day 0), the mice were first treated with 15 mg/Kg biotin *i.p.* or an equivalent volume of PBS, and 8 hours later they received 2.6 mg/kg MTX, 10 mg/kg OXA or an equivalent volume of PBS *i.p.*. Chemotherapy was repeated at day 2, and biotin was injected daily for 2 weeks. For the validation of biotin induced SBP-mtCALR release, tumors were excised 4 or 8 hours after biotin injection and immediately fixed in 4% PFA before being embedded in O.C.T and frozen at -80°C. The tissue was sectioned, permeabilized with 0.5% Triton X-100 and stained with SBP antibody followed by Alexa Fluor 568-conjugated anti-mouse secondary antibody. Images were captured with an HR-SP8 confocal microscope (Leica Biosystems, Wetzlar, Germany). Image analysis was performed with the LAS X software (Leica). For tumor growth assessment, tumor surface was measured regularly and animals bearing neoplastic lesions that exceeded 250 mm^2 were euthanized.

***In vivo* RUSH assay established through hydrodynamic tail vein injection.** For the *in vivo* expression of the RUSH elements Str-KDEL and SBP-ss-GFP, mice were injected intravenously with cDNA (90 µg pCDH-Str-KDEL for the expression of the hook, and 30 µg pCDH-SBP-ss-GFP for the expression of the reporter) in 37°C pre-warmed normal saline of a volume that equals 10 % of the body weight (*e.g.* 2 mL for a mouse with 20 g body weight) via the tail vein. DNA

injection was completed in less than 5 sec. Forty-eight hours after the hydrodynamic injection; mice were either treated with 15 mg/Kg biotin *i.p.*, or equivalent vehicle solutions, for 6 hours before being euthanized to harvest the livers that were subjected to frozen sectioning as described above. Tissue sections were permeabilized with 0.5% Triton X-100 and stained with an anti-streptavidin antibody followed by the Alexa Fluor 647-conjugated anti-mouse secondary antibody. Next, the stained samples were mounted with mounting media containing DAPI and Alexa Fluor™ 568 Phalloidin (Invitrogen). Images were captured with an HR-SP8 confocal microscope (Leica Biosystems). Image analysis was performed with the LAS X software (Leica).

MDSC subsets from mouse peripheral blood mononuclear cells (PBMC) and spleen. Phenotyping of M-MDSC and G-MDSC was performed by flow cytometry. Peripheral blood and spleens were obtained from WT or CALRdel52 mice bearing either naïve MCA205 tumors, MCA205 CALRdel5 tumors, MCA205 CALRins5 tumors, or the MCA205 RUSH tumors (either or not treated by biotin for a week as described above) mice. PBMCs from whole blood were isolated by Ficoll (GE Health Care) gradient centrifugation, and spleens were dissociated as described above. PBMCs and splenocytes were first stained with a Live/Dead Yellow dye to discriminate viable cells, and anti-mouse CD16/32 antibody to block Fc receptors, followed by a staining with anti-CD11b pacific blue, anti-Ly6C FITC Percp, anti-Ly6G PE, antiCD45 APC/eFluor780 for flow cytometric analysis (BD LSRFortessa, BD Biosciences). For the gating of MDCS subpopulations, live $CD45^+$ cells were selected (upon live/dead yellow dye) after exclusion of doublets (based on FSC and SSC). M-MDSCs were defined as $CD11b^+Ly6C^{hi}$ $Ly6G^{lo}$ and G-MDSCs were defined as $CD11b^+Ly6G^{hi}Ly6C^-$ population.

Phenotyping of tumor infiltrating DCs and T cells. ZsGreen-expressing MCA205 cells (either wild type or *Calr* mutant) were inoculated into the right flank of WT C57Bl/6 mice (8 x 10^5/mouse in 100 µL PBS). When tumors became palpable (day 0), the mice were treated with

2.6 mg/kg MTX or an equivalent volume of PBS i.*p.*, at day 0 and 2, and then tumors were harvested at day 10. Viable single cell suspensions were obtained by digesting the tumor (minced to 1~3 mm^3 with scalpels) with collagenase IV (1 mg/mL) and DNase I (50,000 unites/mL). Cells equal to 50 mg tissues were first stained with a Live/Dead Yellow dye and the anti-CD16/CD32 antibody as described above. For the analysis of DC, the samples were further stained with anti-CD11c PE/Cy7, anti-CD80 Percp/Cy5.5, anti-MHC II APC, and antiCD45 APC/eFluor780 antibodies before fixation. For the analysis of T cells, the samples were further stained with anti-CD3 APC, anti-CD4 eFluor450, anti-CD8 AlexaFluor 594, anti-CD25 PE/Vio770, and anti-CD45 APC/eFluor780 antibodies, before they were fixed and permeabilized with the eBioscience™ Foxp3 / Transcription Factor Staining Buffer Set for the staining of anti-FOXP3 FITC antibody. Flow cytometry acquisition was performed on a BD LSRFortessa cytometer, and data analysis was performed with the FlowJo software. After exclusion of doublets and debris, DC were gated according to the expression of CD45, CD11c, CD80, and MHC II, and ZsGreen positive DC were regarded as phagocytosis events. To analyze T cell infiltration, CD3 were used as primary marker of lymphocytes, and the $CD8^+$ cells represent cytotoxic T cells, while $CD4^+CD25^+FOXP3^+$ cells represent regulatory T cells (Tregs).

Patients

All patients were from the Gustave Roussy Cancer Center (Villejuif, France). The study was approved by the institutional Ethics Committee. Plasma of 52 MPN patients or healthy volunteers were prepared via common procedure, and CALR levels were measured with a human calreticulin ELISA kits (RayBiotech) following the manufacture's protocol. PBMCs from whole blood of MPN patients bearing CALR mutations or healthy volunteers were isolated by Ficoll gradient centrifugation. One million PBMCs from each sample were washed with cold PBS, blocked in 1% BSA in PBS before incubation with 100 µL of CALR antibody diluted 1/100 in

PBS containing 1% BSA) for 45 min at 4 °C. Then cells were washed with PBS and further incubated with an Alexa Fluor® 488 goat-anti-rabbit 2nd antibody for additional 30 minutes at 4 °C in the dark. Finally, cells were washed and stained with DAPI before being subjected to flow cytometric analysis.

METHOD DETAILS

Generation of RUSH cell lines

U2OS cells or HeLa cells were infected with Str-KDEL lentiviral particles that were produced using the ViraPower™ lentiviral packaging mix (Thermo Fisher Scientific, Waltham, MA, USA) following the manufacturer's protocol. Transduced cells were pre-selected with G418 (0.5 mg/mL) for 2 weeks, and then single cell sorted by an FACS ARIA III cytofluorometer (Becton Dickinson, San José, CA, USA) for generating U2OS Str-KDEL expressing clones. Clones were validated by additional immunofluorescence staining for streptavidin localization. The hook cell lines were further transduced by means of the ViraPower™ lentiviral expression system (Thermo Fisher Scientific) with the following reporters: SBP-GFP-wtCALR, SBP-GFP-mt1CALR or SBP-GFP-mt2CALR. Transduced cells were pre-selected with hygromycin (0.25 mg/mL) for 2 weeks, and then single cell sorted by an FACS ARIA III cytofluorometer (Becton Dickinson) for generating U2OS cells co-expressing Str-KDEL with SBP-GFP-wtCALR, SBP-GFP-mt1CALR or SBP-GFP-mt2CALR. MCA205 cells co-expressing Str-KDEL with SBP-wtCALR, SBP-mt1CALR, SBP-mt2CALR, SBP-CALR$_{delKDEL}$, SBP-CALR$_{E405*}$, or SBP-CALR$_{X352}$ were generated following the same procedure and clones for *in vivo* assay were selected based on the efficacy of the release of reporters in response to biotin.

Mutagenesis of the plasmids by means of the Agilent QuickChange Lightening Assay

Plasmid mutagenesis (deletion or site mutations) was conducted with the QuickChange Lightening Site-directed Mutagenesis kit (Agilent Technologies, Santa Clara, CA, USA), with primers designed by means of the Agilent Primer Design Program (https://www.agilent.com/store/primerDesignProgram.jsp). PCR analysis was conducted according to the manufacture's instruction. Briefly, the pCDH-SBP-CALR$_{delKDEL}$, pCDH-SBP-CALR$_{E405*}$, and pCDH-SBP-CALR$_{X352}$ vectors were generated based on the pCDH-SBP-wtCALR by PCR with primers listed in **Table S1**, using a melting time of 5 mins/cycle; and the pLC-ZsGreen-blast plasmid were generated based on the pLC-ZsGreen-P2A-blast plasmid (Addgene #123322) (Patil et al., 2018) with primers listed also in **Table S1**, using a melting time of 4 mins/cycle. All clones used for transfection were sequence-verified.

CRISPR/Cas9-mediated *Calr* mutations

For the generation of CRISPR-mediated *Calr* mutations, we designed the gRNA (sequence AGAGGACAAGAAGCGTAAAG for type I CALR mutation (*del52)* and the X352 mutation; sequence AGAAGAAGCTGAGGATAAAG for type II (i*ns5*) and the E405* mutation by using the webtool developed by the Zhang lab (http://crispr.mit.edu/). Oligonucleotides containing the above sequence were synthesized (Sigma) and ligated into the pX458 backbone (Addgene #48138, (Ran et al., 2013)) for co-transfection with homology templates containing the mutation sites (synthesized by Invitrogen GeneArt Gene Synthesis (Thermo Fisher Scientific, Inc.). The co-transfection was performed by means of lipofectamine 3000 (Thermo Fisher Scientific, Inc.) following the manufacture's protocol. Forty-eight hours after transfection, GFP-positive cells were sorted into single cells before surviving clones were expanded for genomic DNA extraction. The targeted region in genomic DNA was amplified by PCR using the Phusion® High-Fidelity PCR Master Mix (New England BioLabs; Ipswich, MA, US) with primers 5'

ccgggacaatctttgacaat 3' and 5' gtgttcaggcctcagtcca 3', and purified with the Monarch® DNA Gel Extraction Kit (New England BioLabs) before being sent to Eurofins Genomics GmbH (Bersberg, Germany) for sequencing with the primer 5' ggcctatgcagaggagtttg 3'. Positive clones were expanded and subjected to DNA extraction for sequence validation.

Western blotting

Protein was precipitated from cell culture supernatants by the addition of cold acetone (-20 °C, 4x v/v) and the agitation at 4°C overnight, followed by centrifugation at 5,000 g for 10 min at 4°C. Precipitate and cells were lysed in RIPA lysis buffer containing protease inhibitor cocktail (Roche, Basel, Switzerland), and then total protein content was quantified by mean of a BCA protein assay kit (Thermo Fisher Scientific). Twenty µg of protein was used for SDS PAGE (Invitrogen) and then transferred to PVDF membranes (Merck Millipore). Membranes were blocked in 5% non-fat dry milk/TBST (TBS + 0.01% Tween-20) for 1 h, and incubated with primary antibody overnight at 4°C on a rocking shaker. Membranes were then washed five times with TBST for 10 min each, followed by incubation with secondary antibody for 2 h. Then the membranes were washed with TBST and peroxidase activity was visualized using ECL Prime Western Blotting Detection Reagent (GE Healthcare, Chicago, Il, USA) and an ImageQuant LAS4000 (GE Healthcare).

Immunoprecipitation (IP) assay

Cells were seeded in 75 cm^2 tissue culture flasks (Corning) and let adapt for 24 hours (to get 10^7 cells/flask). Then the medium was replaced with 5 mL serum-free medium and the cells were kept in culture overnight. Supernatant was collected and mixed with 200 mL Pierce® Protein A Agarose beads (Thermo Fisher) and 5 µg rabbit-anti-CALR antibody followed by incubation at 4 °C for 24 h on an orbital shaker. Then the mixture was centrifuged for 3 minutes at 2,500 g and the beads were washed three times with IP buffer (25 mM Tris, 150 mM NaCl; pH 7.2). The

complex-bound resin was washed once more with 0.5 mL of water and resuspended with 50 µL 1X protein electrophoresis loading buffer, boiled at 100°C and centrifuged at 2,500 g to collect the supernatant for SDS-PAGE. As control adherent cells were harvested by trypsinization and lysed to extract intracellular protein for SDS-PAGE. Calreticulin was detected with a chicken-anti-calreticulin antibody.

Immunofluorescence

Cells were seeded in 96 or 384 well black imaging microplates (Greinerbioone, Kremsmünster, Austria) by means of a Multidrop automatic dispenser (Thermo Fisher Scientific) and incubated for 24 h before further treatment. After the treatment, the cells were washed twice with PBS, fixed with 4% PFA for 10 min, and again washed twice with quenching solution (2.67 g/L NH_4Cl in PBS, pH 7.4) for 5 min. Cells were permeabilized for 10 min with 0.1% Triton-X100 in PBS, and rinsed twice with PBS. Then unspecific binding was blocked with 1% BSA in PBST (PBS + 0.01% Tween-20) for 30 min before the incubation with primary antibodies for 45 min. Then cells were rinsed twice with PBS and then incubated with secondary antibodies for 30 min before the addition of Hoechst 33342 (at a final concentration of 2 µg/mL) for another 10 min. After 3 additional washing steps PBS was added. The cells were subjected to automated image acquisition and subsequent image analysis. For automated fluorescence microscopy, a robot-assisted Molecular Devices IXM XL BioImager (Molecular Devices, Sunnyvale, CA, USA) was used to acquire at least 4 view fields of each well. Images were processed using the MetaXpress software (Molecular Devices).

Sandwich ELISA

High binding 96 well plates (Corning) were coated with antibody using the following procedure: 200 µL/well of anti-SBP capture antibody, diluted in PBS at a final concentration of 0.5 µg/mL, was added and incubated for 2 h at 37 °C. The plate was rinsed twice with washing buffer (0.05%

Tween 20 in PBS) before the addition of 100 µL sterile blocking buffer (2% BSA, 0.05% Tween 20 in PBS) to each well and after incubation for 2 h at RT. The blocking buffer was exchanged with 100 µL sterile reaction buffer (1% BSA, 0.05% Tween 20 in PBS) before the addition of 10 µL of sample or standard in each well. Supernatants from cells resuspended in PBS, lysed by sonication and centrifuged at 1500 g for 10 minutes at 4 °C before were used as standards.

Plates were incubated overnight at 4 °C and then rinsed 3 times with washing buffer before the addition of 100 µL of anti-CALR detection antibody, diluted to 1 µg/mL in reaction buffer. Plates were incubated for 2 h at RT, rinsed 3 times with washing buffer, and incubated for 1 h at RT with 100 µL of HRP-conjugated goat-anti-rabbit secondary antibody diluted 1/5000 in reaction buffer. Plates were washed 4 times with washing buffer, 100 µL of 1-Step™ Ultra TMB-ELISA substrate solution (Thermo Fisher Scientific) was added and incubated for 10-30 min at RT in the dark until colorizing. Immediately after 50 µL of stop solution (2M H_2SO_4) were added and the absorbance was measured at 450 nm in a SpectraMax I3 microplate reader (Molecular Devices).

Concentration of secreted CALR (SBP-Tagged) proteins from the RUSH cells.

MCA205 cells stably co-expressing streptavidin-KDEL and SBP-CALR (wildtype without KDEL, or mutants Del52, Ins5, E405*, X352) were cultured in 175 cm^2 tissue culture flasks and expanded to 10 flasks under the maintenance of antibiotics (G418 + Hygromycin B). When cells had grown to 100% confluency, they were washed 3 times with serum-free DMEM, and incubated with 10 mL serum-free DMEM containing 1 mM biotin at 37°C for 12 hours. The supernatants were then collected, centrifuged for 10 min at 3,000 g, and passed through 0.22 µm filters. Protein concentration and buffer exchange were performed by using the Pierce™ Protein Concentrator PES, 10 K MWCO (Thermo Fisher). By centrifuging the columns at 4,000 g, 100 mL protein-containing supernatant was concentrated to <2 mL, which was resuspended in 100

mL PBS. Finally, proteins were concentrated to 1-2 mL. Protein concentrations were quantified by the BCA quantification assay (BioRad), and purity was verified by staining with Ponceau S solution (Sigma) after SDS PAGE and blotting on PVDF membranes.

QUANTIFICATION AND STATISTICAL ANALYSIS

Data mining was performed with the Microsoft Office software package (Microsoft, Redmond, DC, USA). Statistical analysis was performed using GraphPad Prism V7 (GraphPad Software, San Diego, CA, USA). Unless otherwise specified, data are reported as mean ± SEM. Statistical significance was analyzed using the Student's-test. Statistical parameters including the *n* value, the definition of center, and dispersion, precision measures (mean ± SEM) and statistical significance are described in the Figures and Figure Legends. All p values < 0.05 were considered statistically significant. *In vivo* tumor growth and tumor-free survival data was analyzed using the freely available TumGrowth software (https://github.com/kroemerlab/TumGrowth) (Enot et al., 2018).

DATA AND SOFTWARE AVAILABILITY

N/A

Supplemental Information

Supplementary Materials (PDF document): Table S1 and Figures S1–S7.

Data file S1. Related to Figure 6. Source information of CALR mutations identified in myeloproliferative neoplasm and solid tumors.

Movie S1. Related to Figure 1. Real-time imaging of the SBP-EGFP-wtCALR reporter in the absence of BFA pretreatment.

Movie S2. Related to Figure 1. Real-time imaging of the SBP-EGFP-mt1CALR reporter in the absence of BFA pretreatment.

Movie S3. Related to Figure 1. Real-time imaging of the SBP-EGFP-mt2CALR reporter in the absence of BFA pretreatment.

Movie S4. Related to Figure 1. Real-time imaging of the SBP-EGFP-wtCALR reporter in the presence of BFA pretreatment.

Movie S5. Related to Figure 1. Real-time imaging of the SBP-EGFP-mt1CALR reporter in the presence of BFA pretreatment.

Movie S6. Related to Figure 1. Real-time imaging of the SBP-EGFP-mt2CALR reporter in the presence of BFA pretreatment.

References

Araki, M., and Komatsu, N. (2017). Novel molecular mechanism of cellular transformation by a mutant molecular chaperone in myeloproliferative neoplasms. Cancer Sci *108*, 1907-1912.

Araki, M., Yang, Y., Masubuchi, N., Hironaka, Y., Takei, H., Morishita, S., Mizukami, Y., Kan, S., Shirane, S., Edahiro, Y.*, et al.* (2016). Activation of the thrombopoietin receptor by mutant calreticulin in CALR-mutant myeloproliferative neoplasms. Blood *127*, 1307-1316.

Arshad, N., and Cresswell, P. (2018). Tumor-associated calreticulin variants functionally compromise the peptide loading complex and impair its recruitment of MHC-I. J Biol Chem *293*, 9555-9569.

Boncompain, G., Divoux, S., Gareil, N., de Forges, H., Lescure, A., Latreche, L., Mercanti, V., Jollivet, F., Raposo, G., and Perez, F. (2012). Synchronization of secretory protein traffic in populations of cells. Nat Methods *9*, 493-498.

Brown, G.C., and Neher, J.J. (2012). Eaten alive! Cell death by primary phagocytosis: 'phagoptosis'. Trends Biochem Sci *37*, 325-332.

Byrne, J.C., Ni Gabhann, J., Stacey, K.B., Coffey, B.M., McCarthy, E., Thomas, W., and Jefferies, C.A. (2013). Bruton's tyrosine kinase is required for apoptotic cell uptake via regulating the phosphorylation and localization of calreticulin. J Immunol *190*, 5207-5215.

Chachoua, I., Pecquet, C., El-Khoury, M., Nivarthi, H., Albu, R.I., Marty, C., Gryshkova, V., Defour, J.P., Vertenoeil, G., Ngo, A.*, et al.* (2016). Thrombopoietin receptor activation by myeloproliferative neoplasm associated calreticulin mutants. Blood *127*, 1325-1335.

Chao, M.P., Jaiswal, S., Weissman-Tsukamoto, R., Alizadeh, A.A., Gentles, A.J., Volkmer, J., Weiskopf, K., Willingham, S.B., Raveh, T., Park, C.Y.*, et al.* (2010). Calreticulin is the dominant pro-phagocytic signal on multiple human cancers and is counterbalanced by CD47. Sci Transl Med *2*, 63ra94.

Costello, A., Lao, N.T., Gallagher, C., Capella Roca, B., Julius, L.A.N., Suda, S., Ducree, J., King, D., Wagner, R., Barron, N.*, et al.* (2018). Leaky Expression of the TET-On System Hinders Control of Endogenous miRNA Abundance. Biotechnol J, e1800219.

Elf, S., Abdelfattah, N.S., Baral, A.J., Beeson, D., Rivera, J.F., Ko, A., Florescu, N., Birrane, G., Chen, E., and Mullally, A. (2018). Defining the requirements for the pathogenic interaction between mutant calreticulin and MPL in MPN. Blood *131*, 782-786.

Elf, S., Abdelfattah, N.S., Chen, E., Perales-Paton, J., Rosen, E.A., Ko, A., Peisker, F., Florescu, N., Giannini, S., Wolach, O.*, et al.* (2016). Mutant Calreticulin Requires Both Its Mutant C-terminus and the Thrombopoietin Receptor for Oncogenic Transformation. Cancer Discov *6*, 368-381.

Enot, D.P., Vacchelli, E., Jacquelot, N., Zitvogel, L., and Kroemer, G. (2018). TumGrowth: An open-access web tool for the statistical analysis of tumor growth curves. Oncoimmunology *7*, e1462431.

Feng, M., Chen, J.Y., Weissman-Tsukamoto, R., Volkmer, J.P., Ho, P.Y., McKenna, K.M., Cheshier, S., Zhang, M., Guo, N., Gip, P.*, et al.* (2015). Macrophages eat cancer cells using their own calreticulin as a guide: roles of TLR and Btk. Proc Natl Acad Sci U S A *112*, 2145-2150.

Feng, M., Marjon, K.D., Zhu, F., Weissman-Tsukamoto, R., Levett, A., Sullivan, K., Kao, K.S., Markovic, M., Bump, P.A., Jackson, H.M.*, et al.* (2018). Programmed cell removal by calreticulin in tissue homeostasis and cancer. Nat Commun *9*, 3194.

Galluzzi, L., Buque, A., Kepp, O., Zitvogel, L., and Kroemer, G. (2017). Immunogenic cell death in cancer and infectious disease. Nat Rev Immunol *17*, 97-111.
Garbati, M.R., Welgan, C.A., Landefeld, S.H., Newell, L.F., Agarwal, A., Dunlap, J.B., Chourasia, T.K., Lee, H., Elferich, J., Traer, E.*, et al.* (2016). Mutant calreticulin-expressing cells induce monocyte hyperreactivity through a paracrine mechanism. Am J Hematol *91*, 211-219.
Gardai, S.J., McPhillips, K.A., Frasch, S.C., Janssen, W.J., Starefeldt, A., Murphy-Ullrich, J.E., Bratton, D.L., Oldenborg, P.A., Michalak, M., and Henson, P.M. (2005). Cell-surface calreticulin initiates clearance of viable or apoptotic cells through trans-activation of LRP on the phagocyte. Cell *123*, 321-334.
Gardai, S.J., Xiao, Y.Q., Dickinson, M., Nick, J.A., Voelker, D.R., Greene, K.E., and Henson, P.M. (2003). By binding SIRPalpha or calreticulin/CD91, lung collectins act as dual function surveillance molecules to suppress or enhance inflammation. Cell *115*, 13-23.
Garg, A.D., Krysko, D.V., Verfaillie, T., Kaczmarek, A., Ferreira, G.B., Marysael, T., Rubio, N., Firczuk, M., Mathieu, C., Roebroek, A.J.*, et al.* (2012). A novel pathway combining calreticulin exposure and ATP secretion in immunogenic cancer cell death. EMBO J *31*, 1062-1079.
Greives, M.R., Samra, F., Pavlides, S.C., Blechman, K.M., Naylor, S.M., Woodrell, C.D., Cadacio, C., Levine, J.P., Bancroft, T.A., Michalak, M.*, et al.* (2012). Exogenous calreticulin improves diabetic wound healing. Wound Repair Regen *20*, 715-730.
Grinfeld, J., Nangalia, J., Baxter, E.J., Wedge, D.C., Angelopoulos, N., Cantrill, R., Godfrey, A.L., Papaemmanuil, E., Gundem, G., MacLean, C.*, et al.* (2018). Classification and Personalized Prognosis in Myeloproliferative Neoplasms. N Engl J Med *379*, 1416-1430.
Han, L., Schubert, C., Kohler, J., Schemionek, M., Isfort, S., Brummendorf, T.H., Koschmieder, S., and Chatain, N. (2016). Calreticulin-mutant proteins induce megakaryocytic signaling to transform hematopoietic cells and undergo accelerated degradation and Golgi-mediated secretion. J Hematol Oncol *9*, 45.
He, X.Y., Gong, F.Y., Chen, Y., Zhou, Z., Gong, Z., and Gao, X.M. (2017). Calreticulin Fragment 39-272 Promotes B16 Melanoma Malignancy through Myeloid-Derived Suppressor Cells In Vivo. Front Immunol *8*, 1306.
Hong, C., Zhang, T., and Gao, X.M. (2013). Recombinant murine calreticulin fragment 39-272 expands CD1d(hi)CD5+ IL-10-secreting B cells that modulate experimental autoimmune encephalomyelitis in C57BL/6 mice. Mol Immunol *55*, 237-246.
Klampfl, T., Gisslinger, H., Harutyunyan, A.S., Nivarthi, H., Rumi, E., Milosevic, J.D., Them, N.C., Berg, T., Gisslinger, B., Pietra, D.*, et al.* (2013). Somatic mutations of calreticulin in myeloproliferative neoplasms. N Engl J Med *369*, 2379-2390.
Kroemer, G., Galluzzi, L., Kepp, O., and Zitvogel, L. (2013). Immunogenic cell death in cancer therapy. Annu Rev Immunol *31*, 51-72.
Krysko, D.V., Ravichandran, K.S., and Vandenabeele, P. (2018). Macrophages regulate the clearance of living cells by calreticulin. Nat Commun *9*, 4644.
Liu, P., Zhao, L., Loos, F., Iribarren, K., Lachkar, S., Zhou, H., Gomes-da-Silva, L.C., Chen, G., Bezu, L., Boncompain, G.*, et al.* (2017). Identification of pharmacological agents that induce HMGB1 release. Sci Rep *7*, 14915.
Liu, P., Zhao, L., Pol, J., Levesque, S., Petrazzuolo, A., Pfirschke, C., Engblom, C., Rickelt, S., Yamazaki, T., Iribarren, K.*, et al.* (2019). Crizotinib-induced immunogenic cell death in non-small cell lung cancer. Nat Commun *10*, 1486.

Mans, S., Banz, Y., Mueller, B.U., and Pabst, T. (2012). The angiogenesis inhibitor vasostatin is regulated by neutrophil elastase-dependent cleavage of calreticulin in AML patients. Blood *120*, 2690-2699.
Marty, C., Pecquet, C., Nivarthi, H., El-Khoury, M., Chachoua, I., Tulliez, M., Villeval, J.L., Raslova, H., Kralovics, R., Constantinescu, S.N.*, et al.* (2016). Calreticulin mutants in mice induce an MPL-dependent thrombocytosis with frequent progression to myelofibrosis. Blood *127*, 1317-1324.
Michalak, M., Groenendyk, J., Szabo, E., Gold, L.I., and Opas, M. (2009). Calreticulin, a multi-process calcium-buffering chaperone of the endoplasmic reticulum. Biochem J *417*, 651-666.
Nangalia, J., Massie, C.E., Baxter, E.J., Nice, F.L., Gundem, G., Wedge, D.C., Avezov, E., Li, J., Kollmann, K., Kent, D.G.*, et al.* (2013). Somatic CALR mutations in myeloproliferative neoplasms with nonmutated JAK2. N Engl J Med *369*, 2391-2405.
Obeid, M., Tesniere, A., Ghiringhelli, F., Fimia, G.M., Apetoh, L., Perfettini, J.L., Castedo, M., Mignot, G., Panaretakis, T., Casares, N.*, et al.* (2007). Calreticulin exposure dictates the immunogenicity of cancer cell death. Nat Med *13*, 54-61.
Olivieri, N.F., Templeton, D.M., Koren, G., Chung, D., Hermann, C., Freedman, M.H., and McClelland, R.A. (1990). Evaluation of the oral iron chelator 1,2-dimethyl-3-hydroxypyrid-4-one (L1) in iron-loaded patients. Ann N Y Acad Sci *612*, 369-377.
Osman, R., Tacnet-Delorme, P., Kleman, J.P., Millet, A., and Frachet, P. (2017). Calreticulin Release at an Early Stage of Death Modulates the Clearance by Macrophages of Apoptotic Cells. Front Immunol *8*, 1034.
Panaretakis, T., Kepp, O., Brockmeier, U., Tesniere, A., Bjorklund, A.C., Chapman, D.C., Durchschlag, M., Joza, N., Pierron, G., van Endert, P.*, et al.* (2009). Mechanisms of pre-apoptotic calreticulin exposure in immunogenic cell death. EMBO J *28*, 578-590.
Patil, A., Manzano, M., and Gottwein, E. (2018). CK1alpha and IRF4 are essential and independent effectors of immunomodulatory drugs in primary effusion lymphoma. Blood *132*, 577-586.
Pietrocola, F., Pol, J., Vacchelli, E., Rao, S., Enot, D.P., Baracco, E.E., Levesque, S., Castoldi, F., Jacquelot, N., Yamazaki, T.*, et al.* (2016). Caloric Restriction Mimetics Enhance Anticancer Immunosurveillance. Cancer Cell *30*, 147-160.
Ran, F.A., Hsu, P.D., Wright, J., Agarwala, V., Scott, D.A., and Zhang, F. (2013). Genome engineering using the CRISPR-Cas9 system. Nat Protoc *8*, 2281-2308.
Stripecke, R., Carmen Villacres, M., Skelton, D., Satake, N., Halene, S., and Kohn, D. (1999). Immune response to green fluorescent protein: implications for gene therapy. Gene Ther *6*, 1305-1312.
Terai, T., Kohno, M., Boncompain, G., Sugiyama, S., Saito, N., Fujikake, R., Ueno, T., Komatsu, T., Hanaoka, K., Okabe, T.*, et al.* (2015). Artificial Ligands of Streptavidin (ALiS): Discovery, Characterization, and Application for Reversible Control of Intracellular Protein Transport. J Am Chem Soc *137*, 10464-10467.
Vacchelli, E., Ma, Y., Baracco, E.E., Sistigu, A., Enot, D.P., Pietrocola, F., Yang, H., Adjemian, S., Chaba, K., Semeraro, M.*, et al.* (2015). Chemotherapy-induced antitumor immunity requires formyl peptide receptor 1. Science *350*, 972-978.
Vainchenker, W., and Kralovics, R. (2017). Genetic basis and molecular pathophysiology of classical myeloproliferative neoplasms. Blood *129*, 667-679.

van Vliet, A.R., Giordano, F., Gerlo, S., Segura, I., Van Eygen, S., Molenberghs, G., Rocha, S., Houcine, A., Derua, R., Verfaillie, T.*, et al.* (2017). The ER Stress Sensor PERK Coordinates ER-Plasma Membrane Contact Site Formation through Interaction with Filamin-A and F-Actin Remodeling. Mol Cell *65*, 885-899 e886.
Wiersma, V.R., Michalak, M., Abdullah, T.M., Bremer, E., and Eggleton, P. (2015). Mechanisms of Translocation of ER Chaperones to the Cell Surface and Immunomodulatory Roles in Cancer and Autoimmunity. Front Oncol *5*, 7.
Wijeyesakere, S.J., Bedi, S.K., Huynh, D., and Raghavan, M. (2016). The C-Terminal Acidic Region of Calreticulin Mediates Phosphatidylserine Binding and Apoptotic Cell Phagocytosis. J Immunol *196*, 3896-3909.
Zhao, L., Liu, P., Boncompain, G., Loos, F., Lachkar, S., Bezu, L., Chen, G., Zhou, H., Perez, F., Kepp, O.*, et al.* (2018). Identification of pharmacological inhibitors of conventional protein secretion. Sci Rep *8*, 14966.

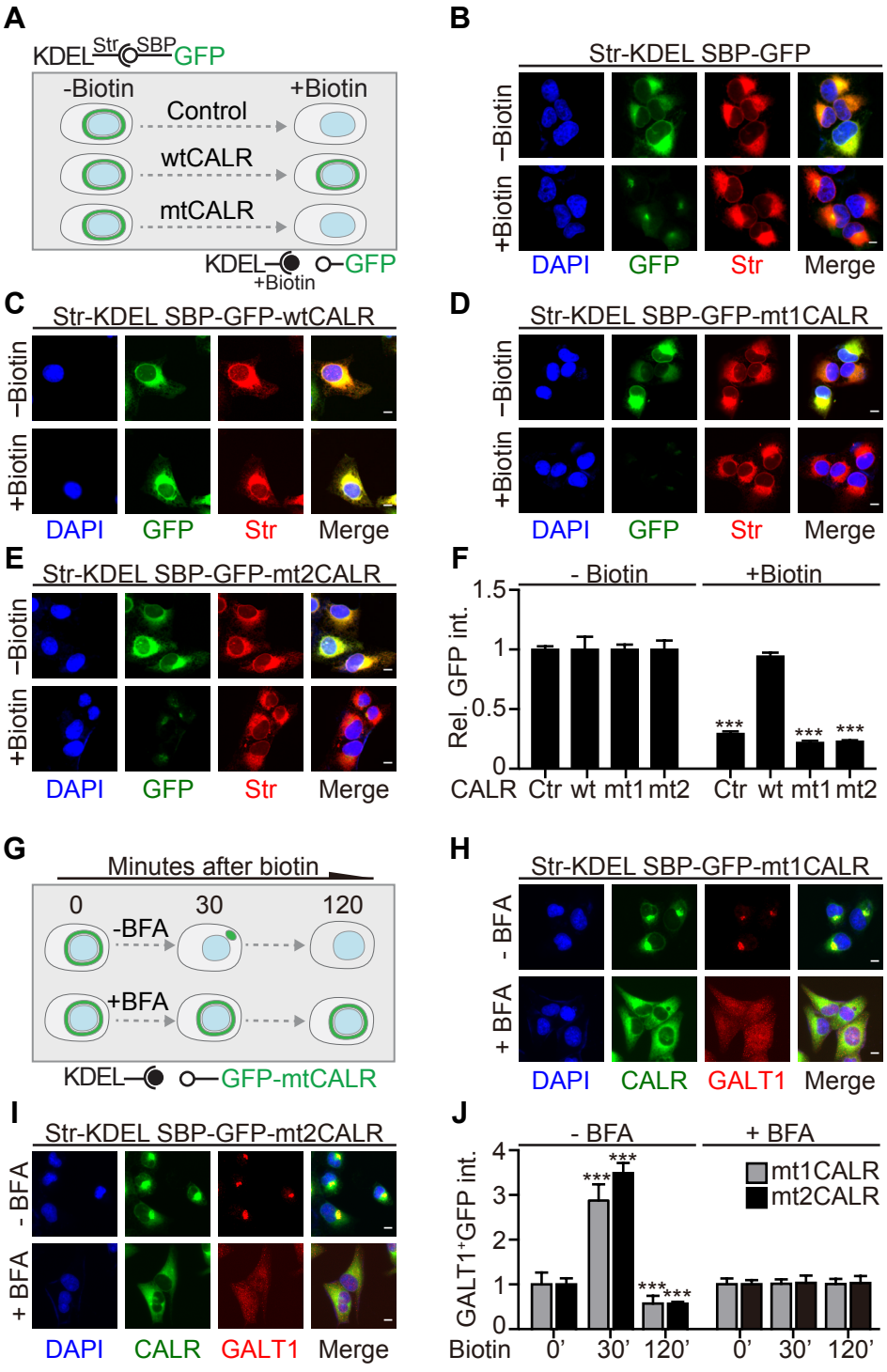
A
KDEL Str SBP GFP
-Biotin
+Biotin
Control
wtCALR
mtCALR
KDEL GFP
+Biotin
B
Str-KDEL SBP-GFP
−Biotin
+Biotin
DAPI
GFP
Str
Merge
C
Str-KDEL SBP-GFP-wtCALR
D
Str-KDEL SBP-GFP-mt1CALR
E
Str-KDEL SBP-GFP-mt2CALR
F
- Biotin
+Biotin
Rel. GFP int.
1.5
1
0.5
0
***
CALR Ctr wt mt1 mt2 Ctr wt mt1 mt2
G
Minutes after biotin
0
30
120
-BFA
+BFA
KDEL GFP-mtCALR
H
Str-KDEL SBP-GFP-mt1CALR
- BFA
+ BFA
DAPI
CALR
GALT1
Merge
I
Str-KDEL SBP-GFP-mt2CALR
J
- BFA
+ BFA
GALT1+GFP int.
4
3
2
1
0
mt1CALR
mt2CALR
Biotin 0’ 30’ 120’ 0’ 30’ 120’

Figure 1

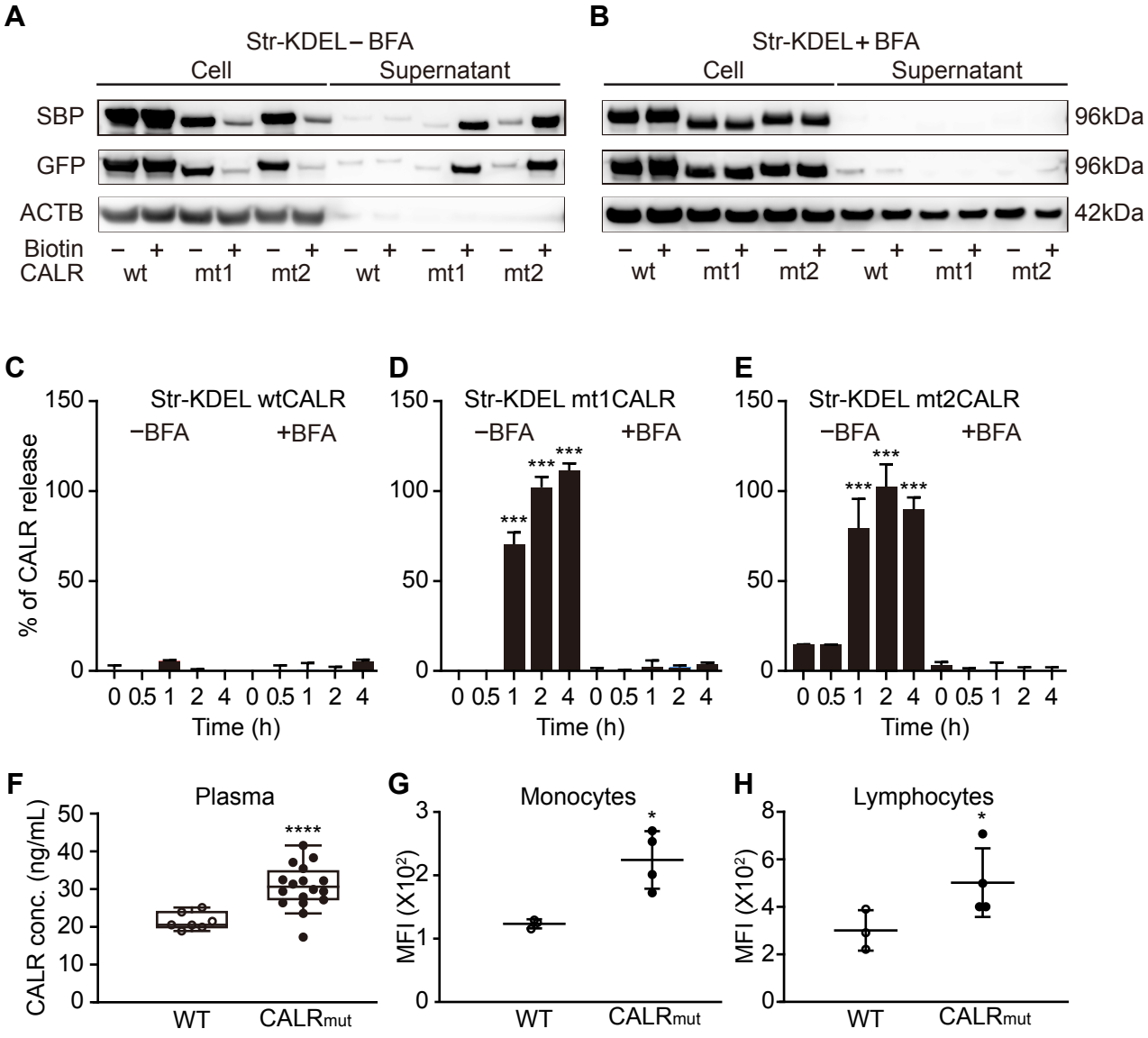
A
Str-KDEL − BFA
Cell
Supernatant
SBP
GFP
ACTB
Biotin
CALR
wt
mt1
mt2
B
Str-KDEL + BFA
96kDa
42kDa
C
Str-KDEL wtCALR
−BFA
+BFA
% of CALR release
Time (h)
D
Str-KDEL mt1CALR
E
Str-KDEL mt2CALR
F
Plasma
CALR conc. (ng/mL)
WT
CALRmut
G
Monocytes
MFI (X10²)
H
Lymphocytes

Figure 2

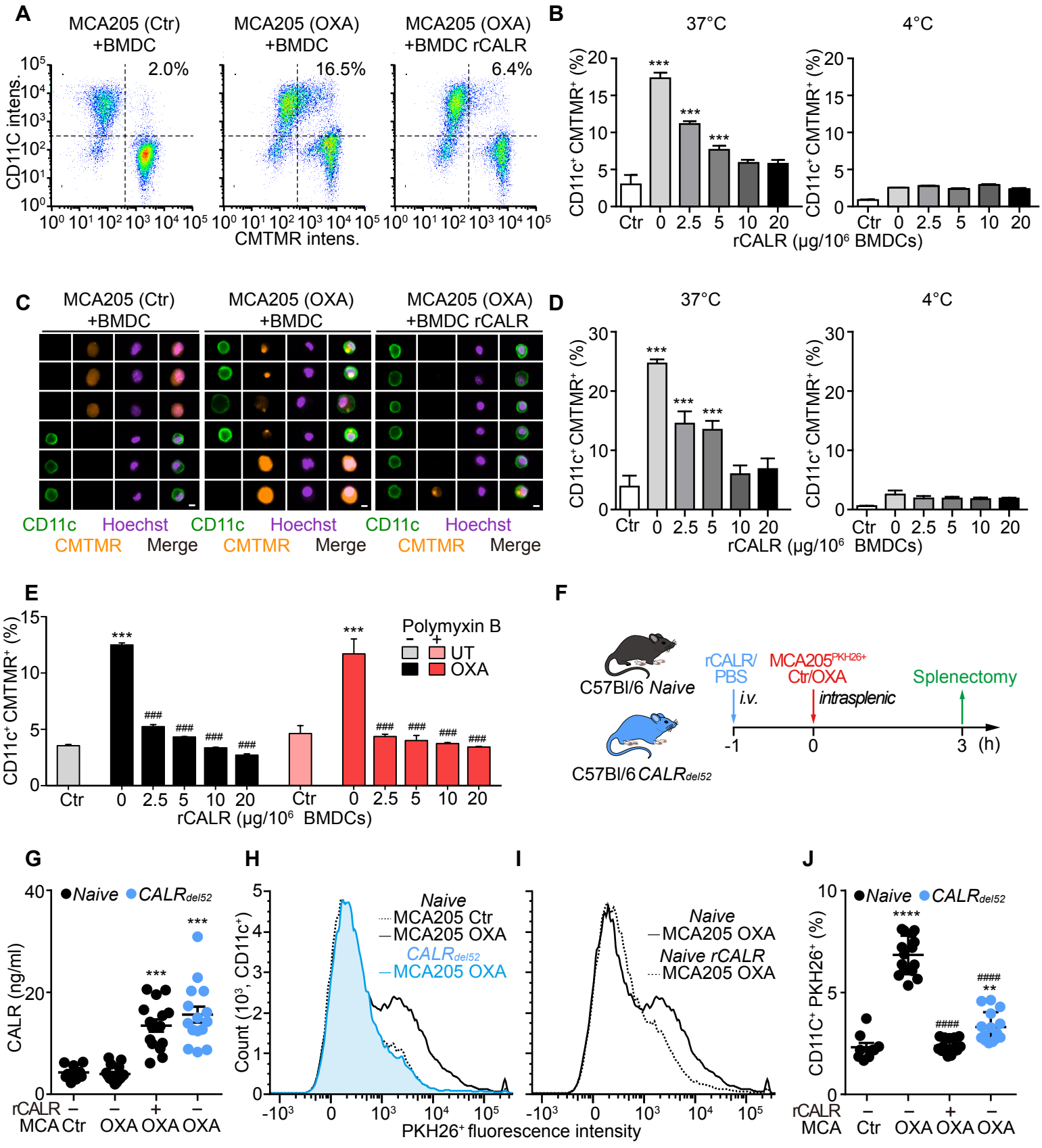
A
MCA205 (Ctr) +BMDC
MCA205 (OXA) +BMDC
MCA205 (OXA) +BMDC rCALR
2.0%
16.5%
6.4%
CD11C intens.
CMTMR intens.
B
37°C
4°C
CD11c+ CMTMR+ (%)
rCALR (μg/10⁶ BMDCs)
C
CD11c Hoechst
CMTMR Merge
D
E
Polymyxin B
UT
OXA
F
C57Bl/6 Naive
C57Bl/6 CALRdel52
rCALR/ PBS
MCA205PKH26+ Ctr/OXA
Splenectomy
i.v.
intrasplenic
(h)
G
Naive
CALRdel52
CALR (ng/ml)
rCALR
MCA Ctr
OXA
H
Naive
MCA205 Ctr
MCA205 OXA
CALRdel52
MCA205 OXA
Count (10³, CD11c+)
PKH26+ fluorescence intensity
I
Naive
MCA205 OXA
Naive rCALR
MCA205 OXA
J
CD11C+ PKH26+ (%)

Figure 3

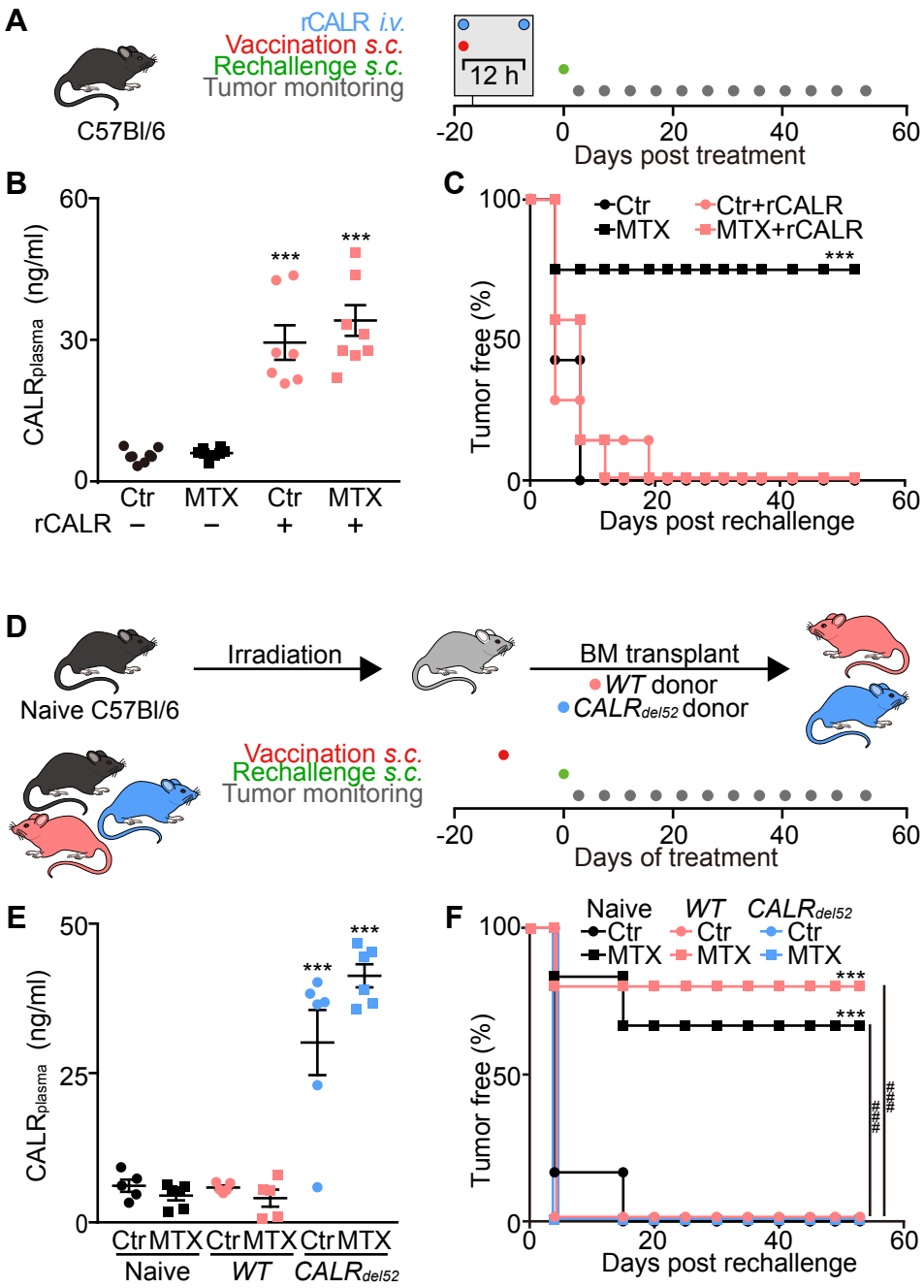
A
rCALR i.v.
Vaccination s.c.
Rechallenge s.c.
Tumor monitoring
C57Bl/6
12 h
-20
0
20
40
60
Days post treatment
B
60
30
0
CALRplasma (ng/ml)
***
***
Ctr
MTX
Ctr
MTX
rCALR
–
–
+
+
C
100
50
0
Tumor free (%)
Ctr
MTX
Ctr+rCALR
MTX+rCALR
***
0
20
40
60
Days post rechallenge
D
Naive C57Bl/6
Irradiation
BM transplant
WT donor
CALRdel52 donor
Vaccination s.c.
Rechallenge s.c.
Tumor monitoring
-20
0
20
40
60
Days of treatment
E
50
25
0
CALRplasma (ng/ml)
***
***
Ctr
MTX
Ctr
MTX
Ctr
MTX
Naive
WT
CALRdel52
F
100
50
0
Tumor free (%)
Naive
WT
CALRdel52
Ctr
MTX
Ctr
MTX
Ctr
MTX
***
***
###
###
0
20
40
60
Days post rechallenge

Figure 4

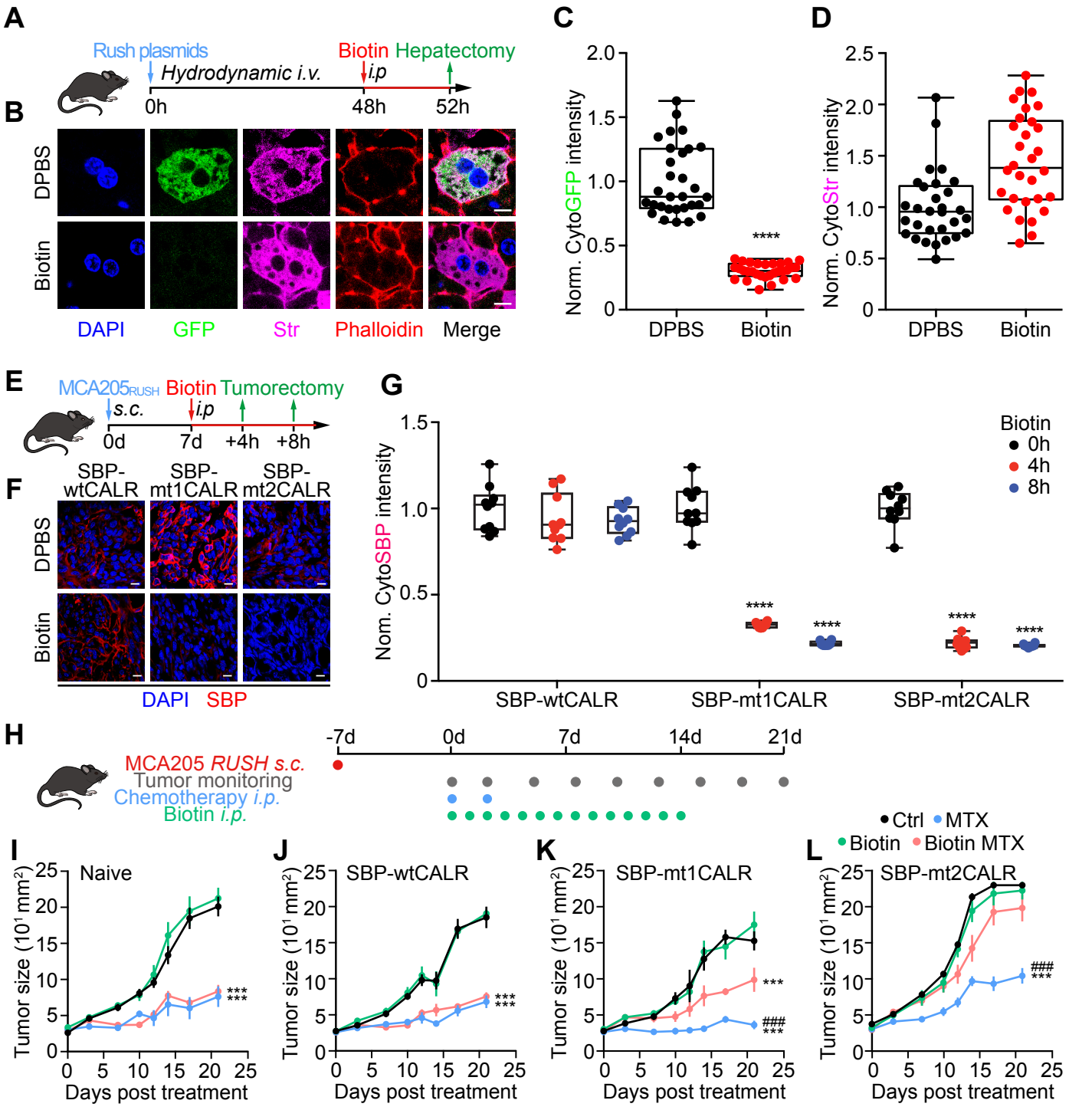
A
Rush plasmids
Hydrodynamic i.v.
Biotin
i.p
Hepatectomy
0h
48h
52h
B
DPBS
Biotin
DAPI
GFP
Str
Phalloidin
Merge
C
Norm. CytoGFP intensity
****
DPBS
Biotin
D
Norm. CytoStr intensity
DPBS
Biotin
E
MCA205RUSH
s.c.
Biotin
i.p
Tumorectomy
0d
7d
+4h
+8h
F
SBP-wtCALR
SBP-mt1CALR
SBP-mt2CALR
DPBS
Biotin
DAPI
SBP
G
Nom. CytoSBP intensity
Biotin
0h
4h
8h
****
SBP-wtCALR
SBP-mt1CALR
SBP-mt2CALR
H
MCA205 RUSH s.c.
Tumor monitoring
Chemotherapy i.p.
Biotin i.p.
-7d
0d
7d
14d
21d
I
Naive
J
SBP-wtCALR
K
SBP-mt1CALR
L
SBP-mt2CALR
Ctrl
MTX
Biotin
Biotin MTX
Tumor size (10¹ mm²)
Days post treatment
***
###

Figure 5

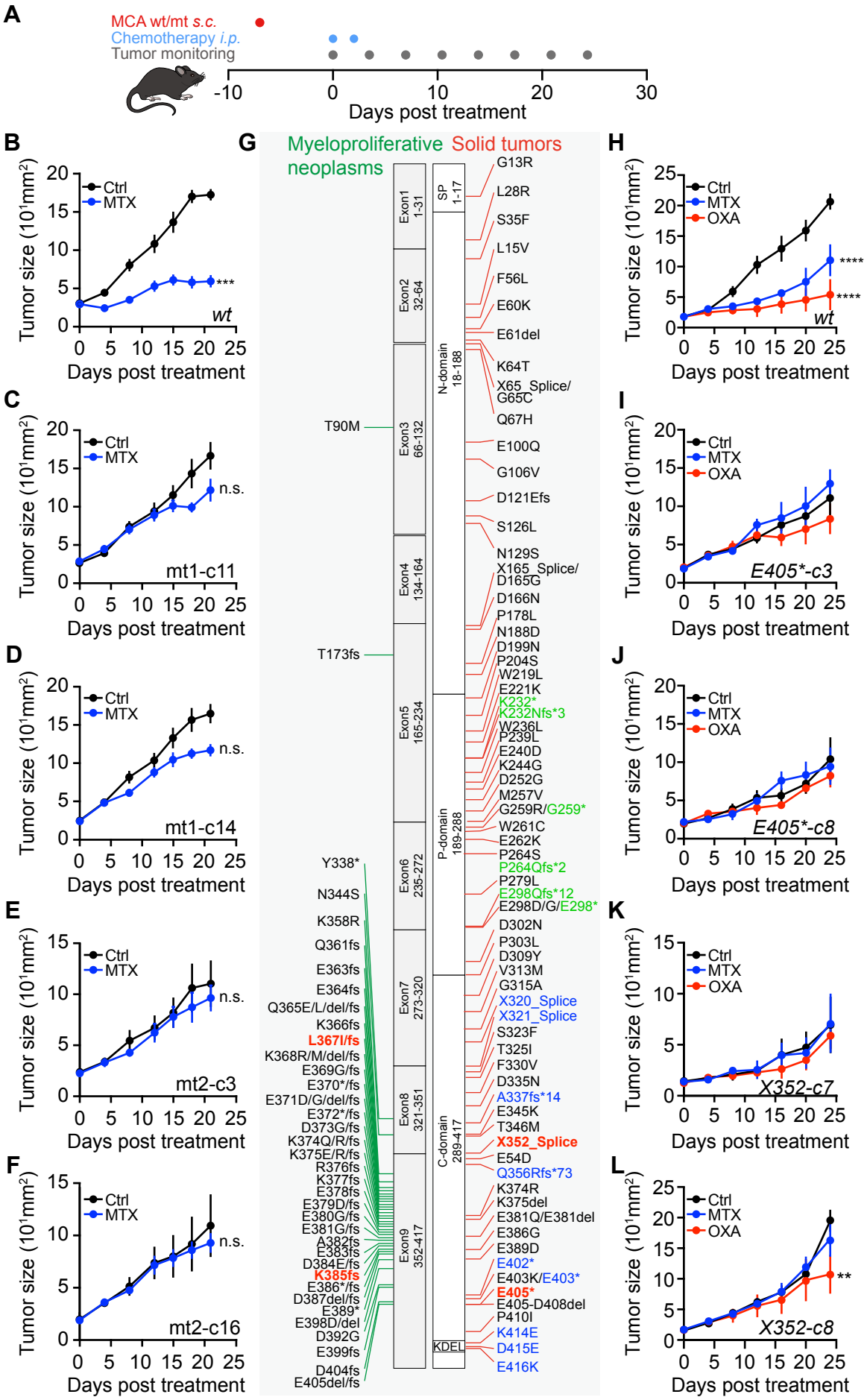
A
MCA wt/mt s.c.
Chemotherapy i.p.
Tumor monitoring
-10
0
10
20
30
Days post treatment
B
Tumor size (10¹mm²)
Ctrl
MTX
***
wt
Days post treatment
C
Ctrl
MTX
n.s.
mt1-c11
Days post treatment
D
Ctrl
MTX
n.s.
mt1-c14
Days post treatment
E
Ctrl
MTX
n.s.
mt2-c3
Days post treatment
F
Ctrl
MTX
n.s.
mt2-c16
Days post treatment
G
Myeloproliferative neoplasms
Solid tumors
Exon1 1-31
Exon2 32-64
Exon3 66-132
Exon4 134-164
Exon5 165-234
Exon6 235-272
Exon7 273-320
Exon8 321-351
Exon9 352-417
SP 1-17
N-domain 18-188
P-domain 189-288
C-domain 289-417
KDEL
T90M
T173fs
Y338*
N344S
K358R
Q361fs
E363fs
E364fs
Q365E/L/del/fs
K366fs
L367I/fs
K368R/M/del/fs
E369G/fs
E370*/fs
E371D/G/del/fs
E372*/fs
D373G/fs
K374Q/R/fs
K375E/R/fs
R376fs
K377fs
E378fs
E379D/fs
E380G/fs
E381G/fs
A382fs
E383fs
D384E/fs
K385fs
E386*/fs
D387del/fs
E389*
E398D/del
D392G
E399fs
D404fs
E405del/fs
G13R
L28R
S35F
L15V
F56L
E60K
E61del
K64T
X65_Splice/ G65C
Q67H
E100Q
G106V
D121Efs
S126L
N129S
X165_Splice/ D165G
D166N
P178L
N188D
D199N
P204S
W219L
E221K
K232*
K232Nfs*3
W236L
P239L
E240D
K244G
D252G
M257V
G259R/G259*
W261C
E262K
P264S
P264Qfs*2
P279L
E298Qfs*12
E298D/G/E298*
D302N
P303L
D309Y
V313M
G315A
X320_Splice
X321_Splice
S323F
T325I
F330V
D335N
A337fs*14
E345K
T346M
X352_Splice
E54D
Q356Rfs*73
K374R
K375del
E381Q/E381del
E386G
E389D
E402*
E403K/E403*
E405*
E405-D408del
P410I
K414E
D415E
E416K
H
Tumor size (10¹mm²)
Ctrl
MTX
OXA
****
****
wt
Days post treatment
I
Ctrl
MTX
OXA
E405*-c3
Days post treatment
J
Ctrl
MTX
OXA
E405*-c8
Days post treatment
K
Ctrl
MTX
OXA
X352-c7
Days post treatment
L
Ctrl
MTX
OXA
**
X352-c8
Days post treatment

Figure 6

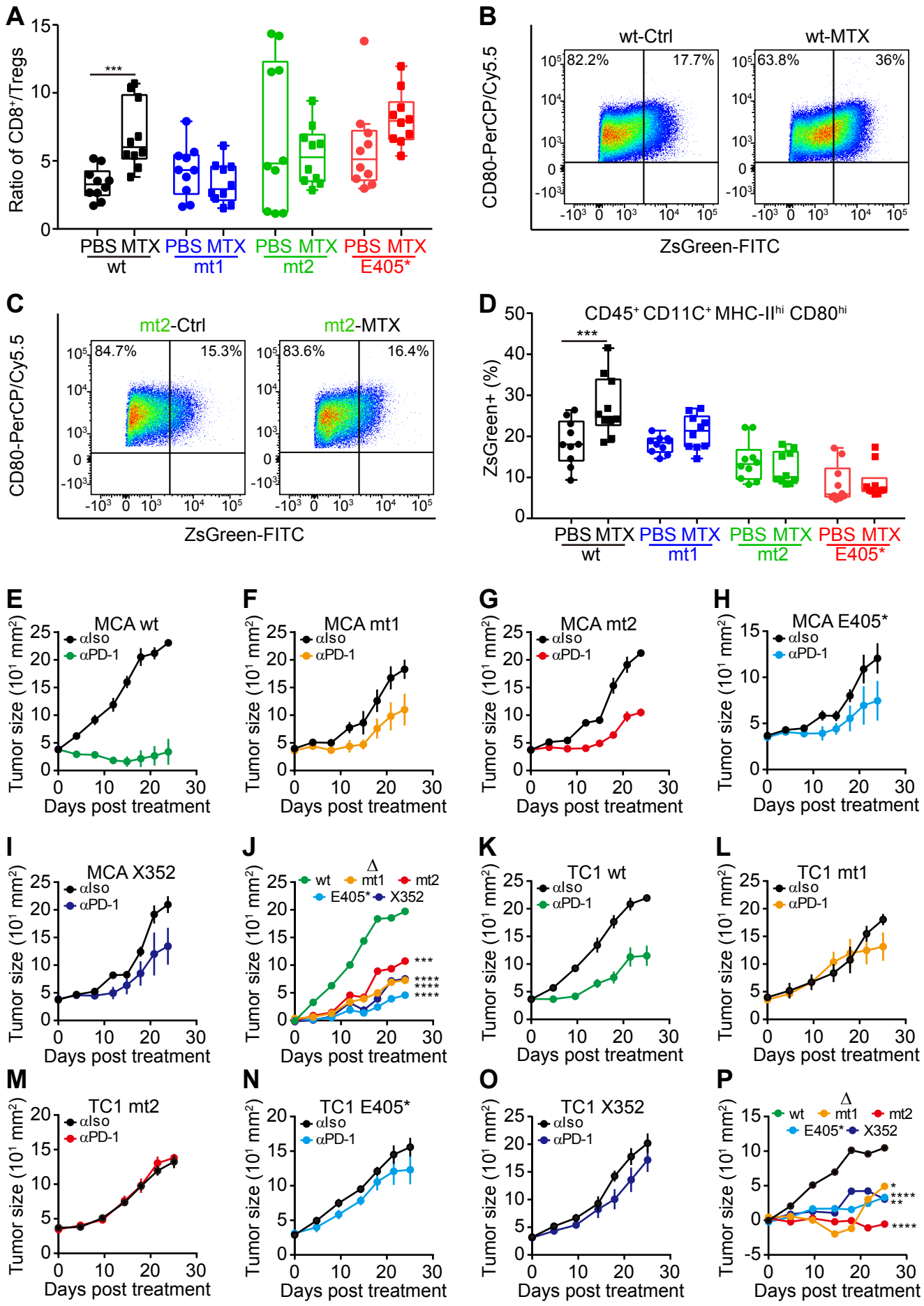
A
Ratio of CD8+/Tregs
***
PBS MTX PBS MTX PBS MTX PBS MTX
wt mt1 mt2 E405*
B
wt-Ctrl
wt-MTX
82.2%
17.7%
63.8%
36%
CD80-PerCP/Cy5.5
ZsGreen-FITC
C
mt2-Ctrl
mt2-MTX
84.7%
15.3%
83.6%
16.4%
CD80-PerCP/Cy5.5
ZsGreen-FITC
D
CD45+ CD11C+ MHC-IIhi CD80hi
ZsGreen+ (%)
***
PBS MTX PBS MTX PBS MTX PBS MTX
wt mt1 mt2 E405*
E
MCA wt
F
MCA mt1
G
MCA mt2
H
MCA E405*
αIso
αPD-1
Tumor size (10¹ mm²)
Days post treatment
I
MCA X352
J
wt mt1 mt2
E405* X352
***
****
****
****
K
TC1 wt
L
TC1 mt1
M
TC1 mt2
N
TC1 E405*
O
TC1 X352
P
wt mt1 mt2
E405* X352
*
****
**
****

Figure 7

Wildtype CALR in cancer cells

Cancer cell

Exposure of truncated CALR by dying cancer cells

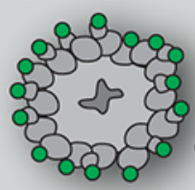

Dying cancer cell

DC efferocytosis of CALR-exposing cancer cells

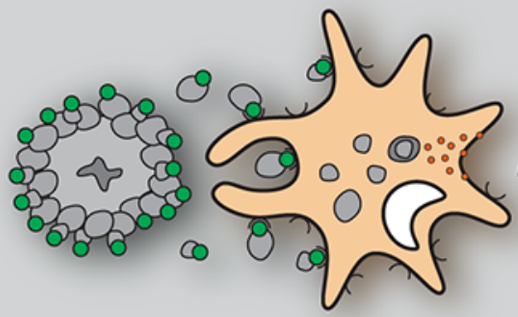

Immature DC

T cell-mediated immunity

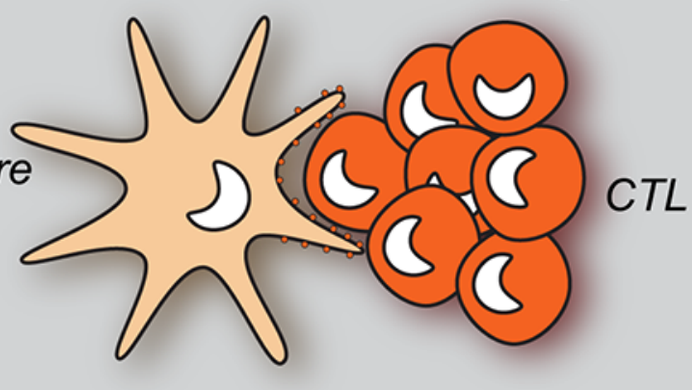

Mature DC

CTL

Truncation mutation of CALR in cancer cells

Secretion of truncated CALR by cancer cells

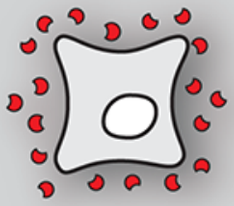

Inhibition of DC efferocytosis of CALR-exposing cancer cells

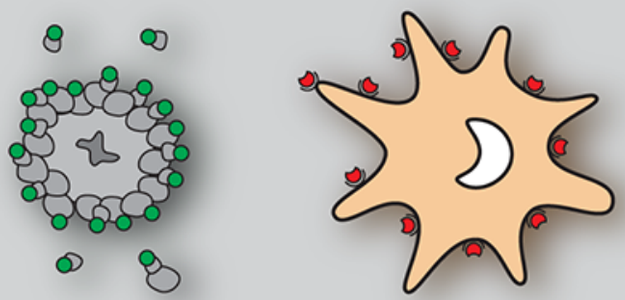

Immunosuppression